Hydrodynamically Modulated Rotating Disk Electrodes

Thesis by

Denice Ball

In Partial Fulfillment of the Requirements

for the Degree of

Master of Science

California Institute of Technology

Pasadena, California

Submitted June 15, 1984

To wimps everywhere . . . . .

Book'em Dano!

ABSTRACT

Hydrodynamically modulated rotating disk electrodes (HMRDE) have been studied and utilized with a basic system. Experimental results follow the theoretical predictions fairly closely with a few exceptions. HMRDE is useful in reducing complications due to background currents. The goal of HMRDE in this report is separation of currents due to surface responses from diffusion controlled currents. Some measure of success was obtained by incorporation of $Ru(NH_3)_6^{3+}$ into a Nafion film. However, the sine wave and square wave modulations are cumbersome and highly inefficient. Once the rotator is interfaced to the IBM 9000H for experimental control and data collection, separation of surface response using HMRDE will be feasible on a practical time scale.

CONTENTS

1. INTRODUCTION

Hydrodynamically modulated rotating disk electrodes (HMRDE) have been studied and utilized with a basic system. Experimental results were compared to theoretical predictions for sinusoidal and square wave modulation with a ferricyanide solution. The HMRDE limitations were checked via experiments involving rate of rotation variation, frequency of modulation variation, and amplitude of modulation variation. Experimental results follow the predictions fairly closely with a few exceptions.

With an aim toward separation of currents due to surface responses from diffusion controlled currents, two systems of modified electrodes were considered. A poly(4-vinyl)pyridine--$Fe(CN)_6^{3-}$ system was abandoned because of apparent loss of adhesion of the polymer coating to the graphite electrode surface. Some measure of success was obtained by incorporation of $Ru(NH_3)_6^{3+}$ into a Nafion film. A surface response current-potential curve was generated by subtracting a RDE scan from a fast-scan RDE (non-steady state). Likewise, subtraction of the HMRDE modulated current from the RDE i-E curve reflecting surface and solution response should result in pure surface response. Point-by-point subtraction resulted in no success, but this failure should not be used as a counter example to disprove the theory of the technique. After this work, the catalytic reduction of oxygen by iron (III) meso-tetraphenylporphine was studied. Once the rotator is interfaced to the IBM 9000H, separation of surface response using HMRDE can be attempted again.

2. THEORY

In electrochemistry, the study of an electron transfer, $O + ne \rightleftarrows R$, involves measuring the current at a working electrode (with respect to a counter electrode) in response to a potential scan or step. Reflected within the total current of an i-E curve are currents due to convection-diffusion, surface reactions, adsorption, double layer charging, solvent electrolysis, and supporting electrolyte interferences. It is often of interest to separate the convection-diffusion current from all others. To obtain reproducible results, one must rigorously control the manner in which reactants are brought to the surface of the electrode. The rotation of an electrode (figure 1) produces a hydrodynamic flow with a well-defined and calculable transport.[1]

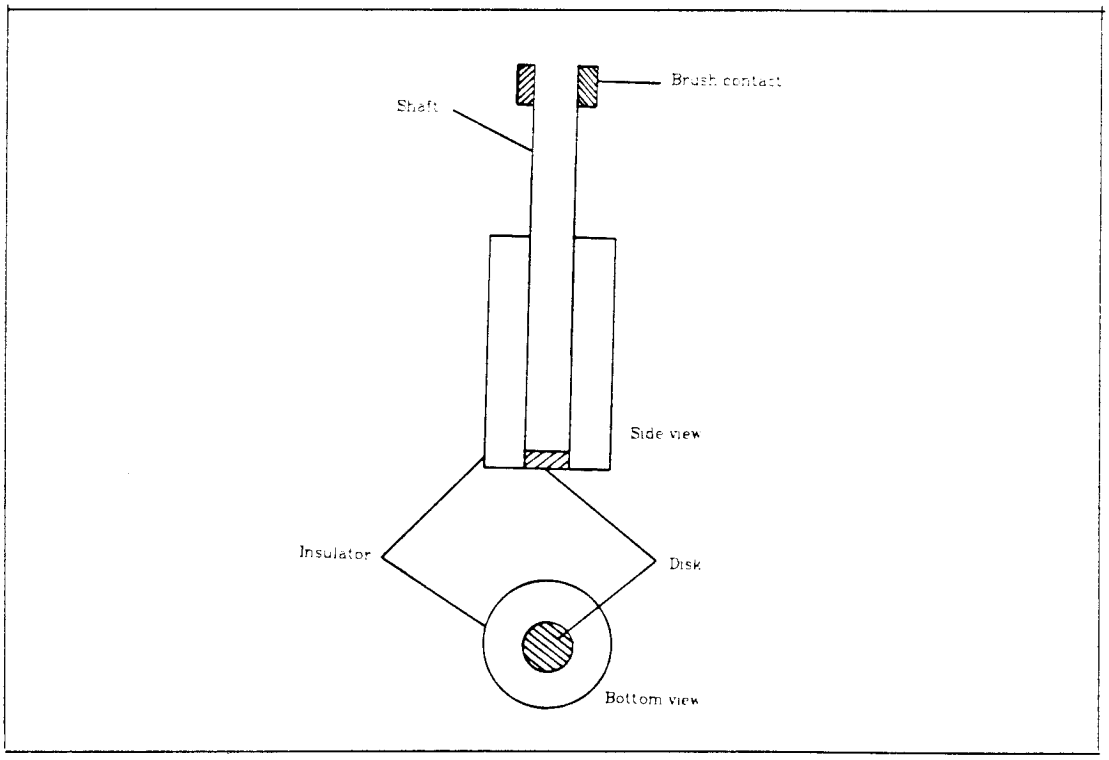

Figure 1: Rotating disk electrode.[2]

The flow diagrams for a well-machined electrode are as expected for the rotation

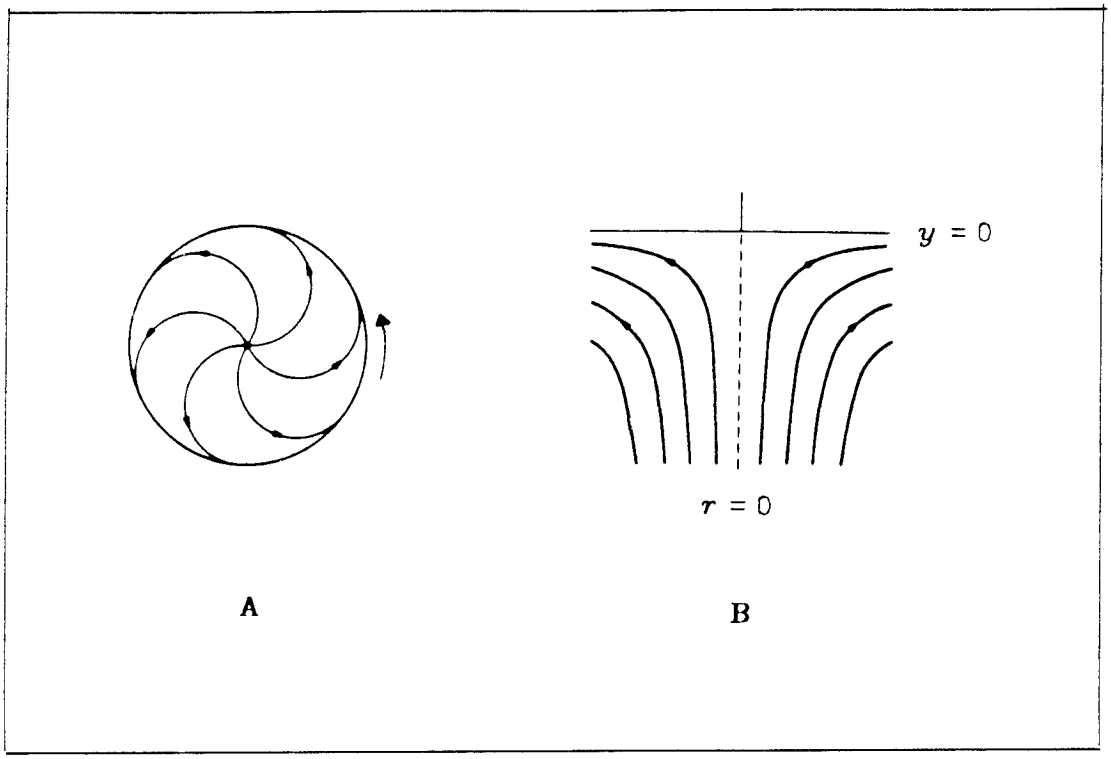

Figure 2: Flow diagram. A) Near the disk surface; B) below the disk surface.[1]

of a cylinder in a liquid (figure 2). Rotation results in a forced convection of the liquid up to the surface of the electrode and out to the sides. At any rotational velocity, a stagnant layer next to the electrode, the hydrodynamic boundary layer, exists and is represented in the concentration profile (figure 3). The thickness of the diffusional layer varies inversely with the rotation rate. Therefore, this method involves forced and reproducible convection of the reactants up to the stagnant layer where diffusion to the electrode surface becomes dominant.

The transport of reactants for the rotating disk electrode (RDE) has been solved or studied by Von Karman, Cochran, Riddiford and Benton.[3] When considering the hydrodynamics, polar coordinates are used (figure 4). The general

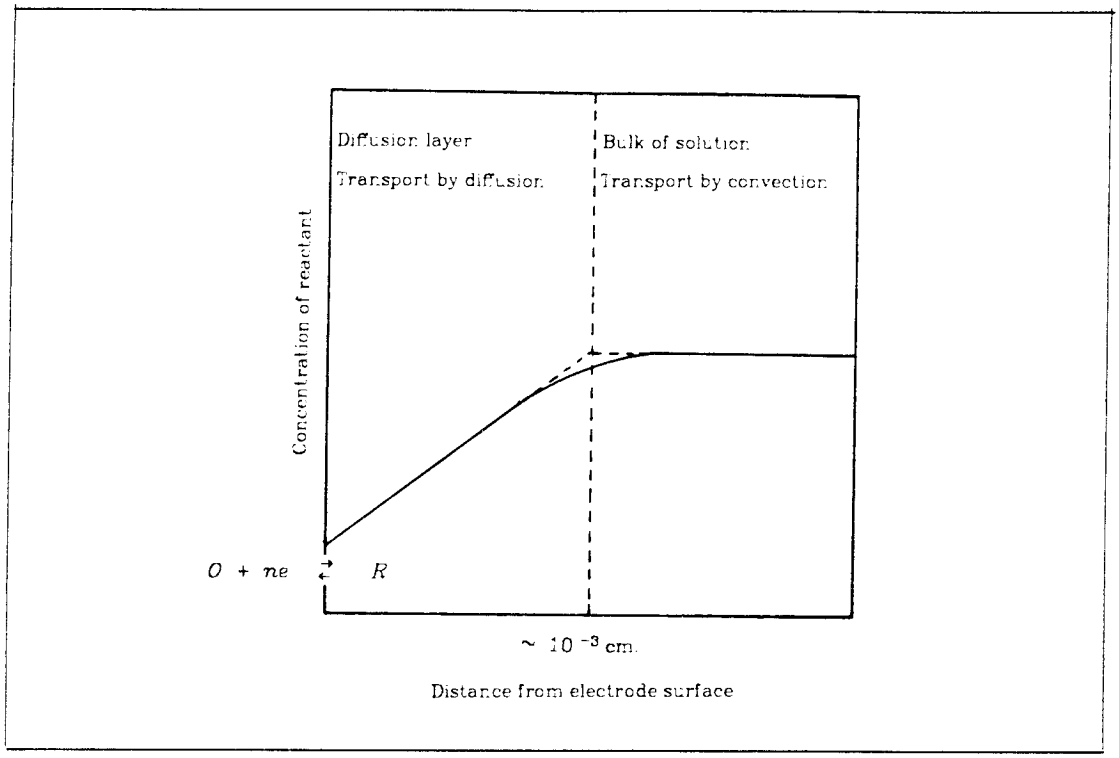

Figure 3: Concentration profile near the surface of an RDE.[1]

convection-diffusion equation in cylindrical coordinates is given by equation 1.

$$\frac{\partial C_o}{\partial t} = D_o\left[\frac{\partial^2 C_o}{\partial y^2} + \frac{\partial^2 C_o}{\partial r^2} + \frac{1}{r}\left(\frac{\partial C_o}{\partial r}\right) + \frac{1}{r^2}\left(\frac{\partial^2 C_o}{\partial \varphi^2}\right)\right] - \left[v_r\left(\frac{\partial C_o}{\partial r}\right) + \frac{v_\varphi}{r}\left(\frac{\partial C_o}{\partial \varphi}\right) + v_y\left(\frac{\partial C_o}{\partial y}\right)\right] \quad (1)$$

where

C_o = concentration of the oxidant at the electrode surface;

D_o = diffusion coefficient of the oxidant.

Figure 5 summarizes the steady-state assumption and other conditions involved in solving the transport.[2]

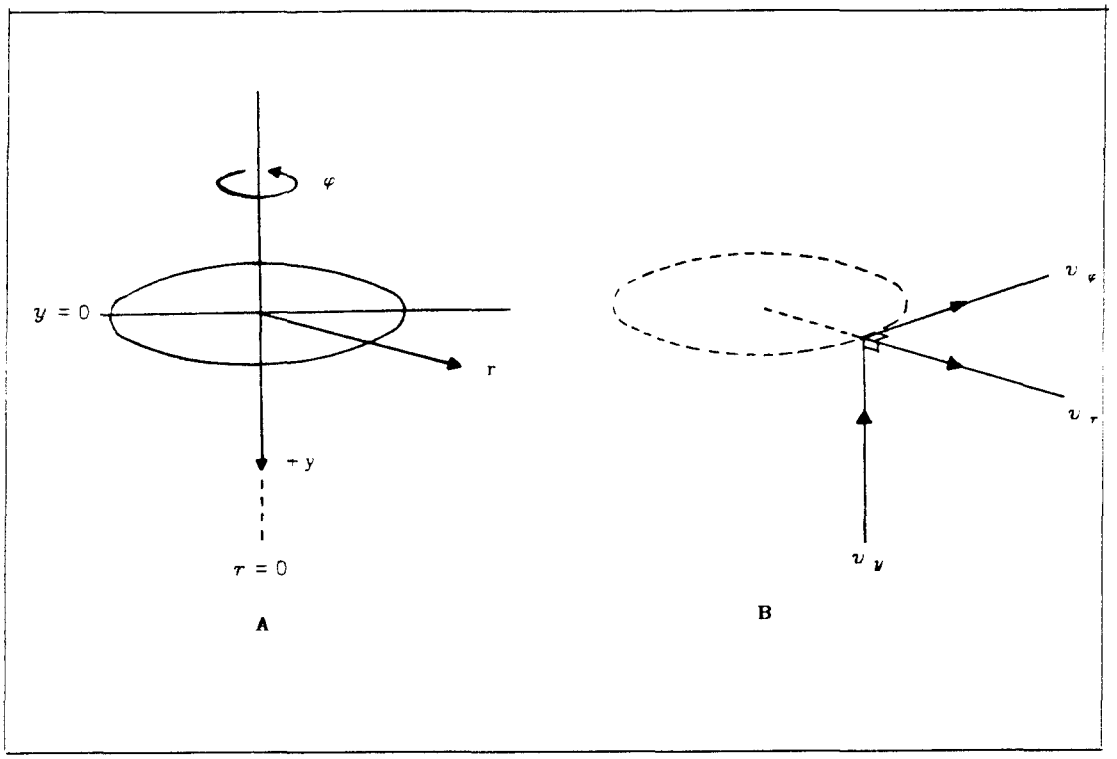

Figure 4: A) Cylindrical polar coordinates; B) velocity components.[1]

When these assumptions and conditions are applied, the convection-diffusion equation reduces to equation 2.

$$0 = D_o \left[\frac{\partial^2 C_o}{\partial y^2}\right] - v_y \left[\frac{\partial C_o}{\partial y}\right] \qquad (2)$$

where

v_y = $-0.51\ \omega^{3/2}\ \nu^{-1/2}\ y^2$;

ω = rotational velocity;

ν = kinematic viscosity.

Equation 2 is rearranged to afford equation 3.

Condition	Explanation
$\frac{\partial C_o}{\partial t} = 0$	Steady-state assumption
$y = 0,\ C_o = 0;\ \lim_{y \to \infty} C_o = C_o^*$	Limiting current condition (C_o^* = bulk concentration of o)
$\frac{\partial C_o}{\partial \varphi} = \frac{\partial^2 C_o}{\partial \varphi^2} = 0$	Symmetry condition
$y = 0,\ 0 < r < r_1;\ \frac{\partial C_o}{\partial r} = \frac{\partial^2 C_o}{\partial r^2} = 0$	Radius condition (r_1 = disk radius)

Figure 5: RDE transport conditions.

$$\frac{\partial^2 C_o}{\partial y^2} = \frac{-y^2}{B}\left[\frac{\partial C_o}{\partial y}\right] \tag{3}$$

where

$$B = (1/0.51)\, D_o\, \nu^{1/2}\, \omega^{-3/2}$$

Integration of equation 3 affords equation 4.

$$C_o^* = \left[\frac{\partial C_o}{\partial y}\right]_{y=0} (0.8934) \left[\frac{3\, D_o\, \omega^{-3/2}\, \nu^{1/2}}{0.51}\right]^{1/3} \tag{4}$$

Combination of equation 4 and the relation given in equation 5 results in the Levich equation (equation 6).[2]

$$i = n\, F\, Ar\, D_o \left[\frac{\partial C_o}{\partial y}\right]_{y=0} \tag{5}$$

$$i_{l,c} = 0.62\, n\, F\, Ar\, D_o^{2/3}\, \omega^{1/2}\, \nu^{-1/6}\, C_o^* \tag{6}$$

where

n = electrons per molecule oxidized or reduced;

F = charge on one mole of electrons;

Ar = area of the disk.

Use of the RDE is based upon the Levich equation. The Levich constant, $i_l/\omega^{1/2}C_o^*$, suggests that one can increase the current obtained by increasing $\omega^{1/2}$ and/or C_o^*.[2] It is important to note that there are limitations upon the rotational velocity. Steady-state assumptions break down if $\omega < 100$ rpm or $\omega > 10000$ rpm. Figure 6 provides a summary of the limitations imposed by the assumptions used to solve the convection-diffusional equations upon the rotating disk experimental conditions.[2]

Criteria	Explanation
$\omega > 10 \frac{\nu}{r_1^2}$	To maintain control over the convective transport
scan rate $<< \omega$	To maintain steady-state assumption
$\omega < 2 \times 10^5 \frac{\nu}{r_1^2}$	To avoid turbulent flow, the Reynolds number must be greater than 2×10^5 ($Re = \omega r_1^2/\nu$)

Figure 6: Limitations on RDE experimental conditions.

Deviations from theory will also be caused by imperfections in the disk surface and in the electrode shaft.

While RDE has advantages over stationary electrochemical methods, complications due to background currents, surface reactions, and charging currents

still arise. Hydrodynamic modulation of the RDE (HMRDE) is a modification which is being used to reduce or eliminate these problems. Miller, Bellavance, and Bruckenstein analyzed both hydrodynamic deviations from steady-state and scan rate dependence for sine-wave and square-wave modulations.[4] Subsequently, Miller, Bruckenstein, and co-workers have concentrated on the sinusoidal hydrodynamic technique, SHM.[5-11] These studies entail experimental verification of theoretical predictions in terms of the electrochemical response of a disk electrode to angular velocity steps, hydrodynamically modulated current-potential curves at the RDE under conditions of mixed electron and mass transfer control, frequency response of limiting currents and electron transfer kinetics. Also, HMRDE has restored the RDE sensitivity limits by eliminating background noise with concentrations as low as 5×10^{-8} M.[7]

Square-wave modulation has been studied and utilized by Blaedel and co-workers.[12,13] A detection limit of 1×10^{-8} M was achieved and rate constants were estimated.[12] In 1981, Wang reviewed HMRDE in terms of theoretical aspects, advantages, disadvantages, and analytical applications.[14] Recent work by Rosamilia and Miller shows that higher amplitudes of modulation produce a proportionate increase in sensitivity.[15] The technique is also being used by Johnson and co-workers to study anodic electrocatalysis.[16] Small transport-controlled currents were separated from the large simultaneous surface-controlled reactions.

In all HMRDE experiments, one pulses the motor from a low rotational speed, ω_1, to a higher rotational speed, ω_2. At each rotational speed, the total current may be viewed as a sum of component currents (equation 7).

$$i_{total} = i_l + i_{nc} + i_{ch} + i_{surf} \qquad (7)$$

where

i_l = convective-diffusion current;

i_{nc} = non-convective component;

i_{ch} = double layer charging current

i_{surf} = surface process current.

The convective-diffusion current, Levich current, is dependent on rotational rate and is expressed in a simplified version of the Levich equation in equation 8.

$$i_l = \kappa_L \omega^{1/2} \tag{8}$$

where

$$\kappa_L = 0.62\ n\ F\ Ar\ D_o^{2/3}\ \nu^{-1/6}\ C_o^*$$

and all other variables are defined as before. The resultant current, Δi, from the step change in rotational rate $\omega_L^{1/2}$ to $\omega_H^{1/2}$ is derived from equations 7 and 8.

$$\Delta i = (\kappa_L \omega_H^{1/2} + i_{nc} + i_{ch} + i_{surf}) - (\kappa_L \omega_L^{1/2} + i_{nc} + i_{ch} + i_{surf}) \tag{9}$$

$$\Delta i = \kappa_L (\omega_H^{1/2} - \omega_L^{1/2}) \tag{10}$$

$$\Delta i = \kappa_L \Delta\omega^{1/2} \tag{11}$$

$$\Delta i = i_H \frac{\Delta\omega^{1/2}}{\omega_H^{1/2}} = i_L \frac{\Delta\omega^{1/2}}{\omega_L^{1/2}} = i_0 \frac{\Delta\omega^{1/2}}{\omega_0^{1/2}} \tag{12}$$

where

$\kappa_L = i_l / \omega^{1/2}$;

$\Delta\omega^{1/2} = \omega_H^{1/2} - \omega_L^{1/2}$;

ω_0 = center rotational rate.

The basic HMRDE assumption for maintenance of hydrodynamic steady-state requires that a plot of Δi vs. $\Delta\omega^{1/2}$ be a straight line with the same slope as a plot of i_l vs. $\omega^{1/2}$ (Levich plot).[7]

When deviations from hydrodynamic steady-state are encountered, the experimental values are adjusted by a dimensionless parameter, the A factor.

$$\Delta i = A\, I_0 \left(\frac{\Delta \omega^{1/2}}{\omega_0^{1/2}} \right) \tag{13}$$

The A factor is a function of:

1. the ratio, p, of the frequency of modulation, f, to the frequency of rotation, ω;
2. the Schmidt number, Sc = kinematic viscosity/D, of electrolyte and electroactive species combination.

The A factor is inversely proportional to both the p factor and the Schmidt number. Tokuda, Bruckenstein, and Miller have derived theoretical values of A and experimentally confirmed them.[8] These tables could be used to determine the diffusion coefficient without knowledge of n or concentration.

For high frequency of modulation, the A factor decreases and accordingly one deviates from the hydrodynamic steady-state. However, the experimental disadvantages include shorter experimental time, easier signal processing, and reduced sensitivity to impurity poisoning. Compensation for reduction in current can be achieved by increasing the amplitude of modulation as shown in equation 14.

$$\text{Sensitivity of response} = \frac{\Delta i}{C_o^{\bullet}\, \omega_0^{1/2}} = A\, \kappa_L^{\bullet} \left(\frac{\Delta \omega^{1/2}}{\omega^{1/2}} \right) \tag{14}$$

where

$$\kappa_L^{\bullet} = 0.62\, n\, F\, Ar\, D_o^{2/3}\, \nu^{-1/6}.$$

The sensitivity of response (a HMRDE equivalent of the Levich constant) in increased by operating at higher $\Delta\omega^{1/2}/\omega^{1/2}$.[15]

In principle, i-E curves might be taken at two rotational speeds and their

difference taken to get a Δi-E curve, showing only the ω-dependent current. This experimental method is limited by the fact that convective and non-convective diffusion controlled currents often change at solid electrodes within the time of two successive experiments.[9] Two possible complications include electrode poisoning due to impurities or electrode geometry changes from surface deposits.

Sine-wave [4-11] and square-wave [12-13] are the types of modulation being investigated and utilized. In sine-wave experiments, one follows the current and modulated current in response to a potential change. The sinusoidal component is obtained from the total current by filtering and passing through a full-wave rectifier. The directly recorded plot of Δi vs. E is valid only if one scans at a slow rate relative to the frequency of modulation. The governing equations are shown below.

$$\omega^{1/2} = \omega_0^{1/2} (1 + \varepsilon \sin \sigma t) \tag{15}$$

$$i(t) = i_{\omega_0} (1 + \varepsilon \sin \sigma t) \tag{16}$$

where

ε = $\Delta\omega^{1/2} / \omega_0^{1/2}$;

σ = frequency of modulation (radians/sec);

t = time;

and all other variables are as defined previously. Sophisticated experimental apparatus, control, and monitoring would allow one to study phase shifts of the sinusoidal Δi response relative to the Δω motor output.

In contrast, square-wave modulation involves pulsing between two rotational speeds while holding the potential at a constant limiting value. This allows direct comparison of current response to motor response. Distortion at

low speeds is caused by hydrodynamic relaxation effects and manifests itself in the rounding of the current wave. For moderate to high speeds, the current wave follows the motor response with no severe deviations. On the opposite end, very high speeds cause distortions due to mechanical rise time limitations and turbulence. Square-wave experiments are useful if obtaining Δi at one potential is sufficient. This method is not a practical manner to obtain Δi vs. E plots because each point must be taken separately.

In conclusion, HMRDE is an effective technique for elimination of interferences that might discourage the use of RDE.[4-16] Sine-wave experiments allow one to record a Δi vs. E curve directly. However, if limiting-currents are sufficient, square-wave experiments are easier to analyze.

3. EXPERIMENTAL

3.1 Chemicals and Reagents

Supporting electrolytes and solutions of the electroactive ions were prepared from commercially available reagent grade salts. $Ru(NH_3)_6Cl_3$ was dissolved in water, reprecipitated with acetone, filtered, and dried under vacuum. All other reagents were used without further purification. Nafion solutions were prepared from a 5% solution of 1100 equivalent weight (CG Processing, Inc.).

Poly(4-vinyl)pyridine (PVP) with a molecular weight of 7.5×10^5 was used. Laboratory distilled water was further purified by passage through a purification train (Barnstead Nanopure). Solutions were deaerated by bubbling with prepurified argon. Oxygen was used without further purification.

3.2 Electrodes

All potentials are reported with respect to a saturated sodium chloride calomel electrode (SSCE). A platinum wire was used as the counter electrode. One of the working electrodes was a commercially manufactured pyrolytic graphite electrode (Pine Instrument Co.). It was polished with alumina on Buhler polishing cloths and the alumina was removed via sonification. Other work was done with a graphite disk that was sealed with heat shrinkable tubing on a steel shaft. The shaft was machined to fit the MSR rotator (Pine Instrument Co.) and the length of tubing was chosen to insulate the portion of the shaft immersed in the electrolyte. The graphite disks were basal plane pyrolytic graphite (BPG; Ar=0.17 cm^2), and edge plane pyrolytic graphite (EPG; Ar=0.36 cm^2) from Union Carbide Co. For BPG electrodes, a fresh electrode surface was prepared by cutting the tubing and the graphite parallel to the electrode surface with a clean razor blade. EPG electrodes were polished and sonicated as described previously.

3.3 Electrochemical Cell

The electrochemical cell was a standard two component cell with a glass frit separating the reference electrode from the working and counter electrodes.

3.4 Polymer-coated Electrodes

Freshly cleaved or polished electrodes were coated with the polymer solution by pipetting μl aliquots to the surface of a horizontally mounted electrode. The solvents were allowed to evaporate from 15 to 60 minutes. Quantities of the reactants incorporated by the polymer coating were measured by transferring an electrode from the loading solution to pure supporting electrolyte and recording the charge vs. time.

3.5 Electrochemical Apparatus

Cyclic voltammetry and RDE were carried out with a PAR Model 173 potentiostat (Princeton Applied Research) driven by a PAR Model 175 programmer. Current-potential curves were recorded with a Houston Instruments 2000 XY recorder. A Pine MSR speed control and motor were used and the rotational velocity was measured with a digital phototachometer (Power Instrument Model 1891-AM). Appendix 1 contains the calibration data for the motor.

3.6 Sine Wave Experiments

The amplitude of the sine wave was adjusted as shown in figure 7. Figure 8 shows the manner in which i_l was followed and Δi was converted to a dc level and recorded. The determination of the conversion factor for the rectifier is detailed in figure 9. The sinusoidal component is obtained from the total current by filtering and passing through a full-wave rectifier. The Δi vs. E and i vs. E curves are recorded as a function of time. To calibrate the equipment and determine the conversion factor, sine waves of known amplitudes (checked with Tektronix scope) were filtered and rectified (figure 9). The data is shown in

Appendix 1 and the conversion factor was determined to be 2.73.

3.7 Square Wave Experiments

The amplitude of the square wave was adjusted as shown in figures 10 and 11. The initial experiments were performed using the set-up in figure 10. Figure 11 is a simplified manner of doing the adjustment. Figures 12 and 13 show the manner in which the current was followed. Once again, initial experiments were done using the set-up detailed in 12 which was later modified into that of figure 13. The rotational rate is switched between two set values and a difference in current is recorded vs. time while a constant applied potential is maintained. For square waves with frequencies of 2 or higher, a Tektronix scope was used to store the wave and transfer it to the XY recorder. This system was calibrated by using square waves of known amplitudes (checked with a voltmeter). The data and calculated conversion factors are shown in Appendix 1.

3.8 Non-steady State RDE Experiments

The solution used was 0.1 M $Ru(NH_3)_6Cl_3$ in 0.2 M CH_3COONa at pH 5.5. For every scan rate at a bare BPG electrode, the lowest rotational rate was determined for which the i-E curve approached steady-state. For this scan rate and rotational rate combination, an i-E curve for a Nafion-coated electrode was recorded. Also, for this rotational rate and a scan rate of 1 mv/sec, an i-E curve for the Nafion-coated electrode was recorded. The difference was taken between the two i-E curves and this difference was compared to the Nafion-coated $Ru(NH_3)_6^{3+}$ response in pure supporting electrolyte.

3.9 Nafion Experiments

Two μl of 0.5% Nafion in isopropanol was micropipetted onto a BPG electrode and allowed to dry for fifteen minutes. The electrode was then soaked in 15 mM $Ru(NH_3)_6^{3+}$. The electrode was transferred to 0.1 mM $Ru(NH_3)_6^{3+}$ solution

(in 0.2 M CH_3COONa at pH=5.5). Continuous cycling was done at 200 mv/sec between potentials of +0.2 and -0.6 volts for 1 hour to stabilize the coating.

3.10 Poly(4-vinylpyridine) Experiments

Two μl of 0.5% PVP in methanol was micropipetted on BPG or EPG electrodes and allowed to dry at least one hour. The electrode was then placed in a solution of $K_3Fe(CN)_6$ (0.2 M CF_3COONa + 0.1 MCF_3COOH). The potential was scanned between +0.6 and -0.6 volts until the polymer was fully loaded (10 minutes).

3.11 Iron(III) meso-tetraphenylporphine (FeTPP) Experiments

A BPG electrode is dipped in a solution of 10^{-4} M FeTPP in methylene chloride and allowed to dry. The electrode is soaked in 0.1 M NaOH for 15 minutes and rinsed with water. The electrode is transferred to a solution of 0.1 M $NaClO_4$ + 0.1 M $HClO_4$. The solution is either bubbled with argon or oxygen for 15 minutes.

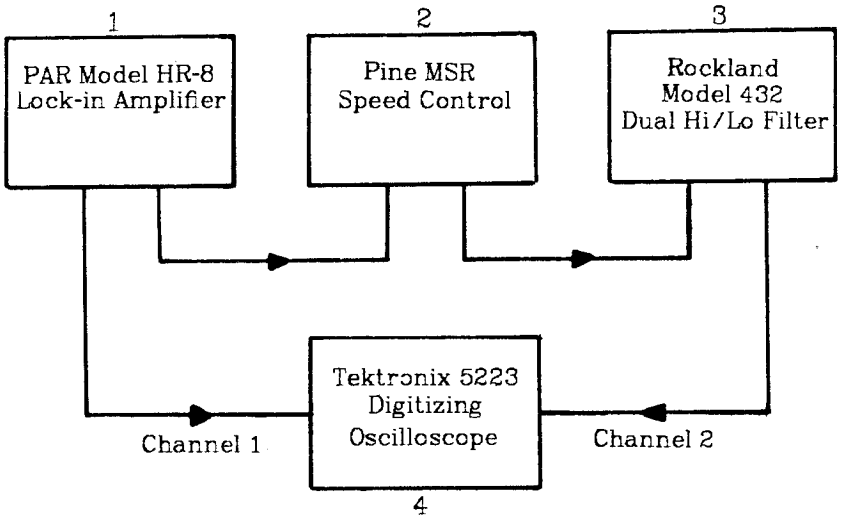

1. Set amplitude and frequency of sine wave (f).
2. Adds sgnal of lock-in amplifier to its setting (1V = 1000 rpm).
3. Filters 2f high and f/2 low.
4. Monitor sine wave that is input to the motor and sine wave of motor output.

Figure 7: Experimental apparatus for amplitude adjustment of sine wave.

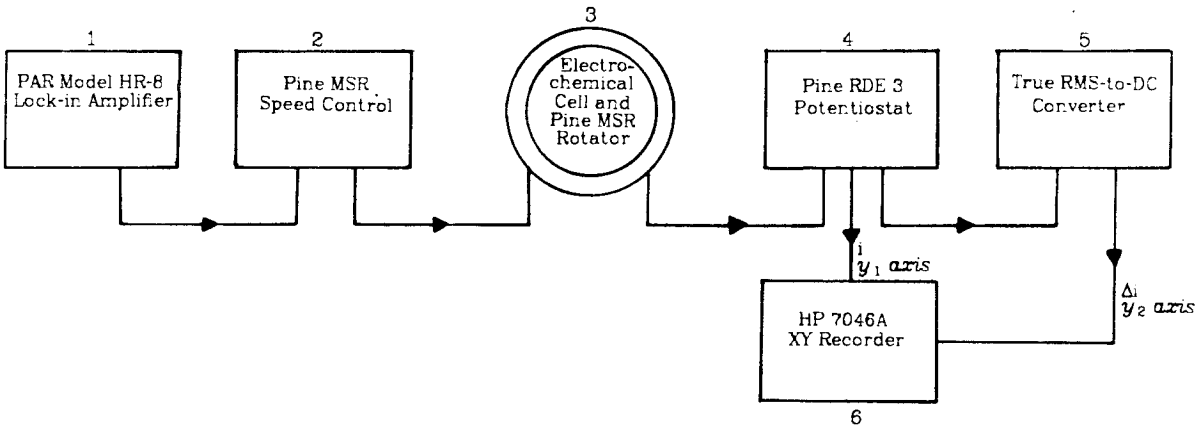

1. Sends sine wave to speed control.
2. Adds signal of lock-in amplifier to its setting (1V = 1000 rpm).
3. Usual functions.
4. Usual functions.
5. Converts AC amplitude to DC level (time constant = 3)
6. Records i and Δi vs potential

Figure 8: Experimental apparatus for monitoring current response in sine wave experiments.

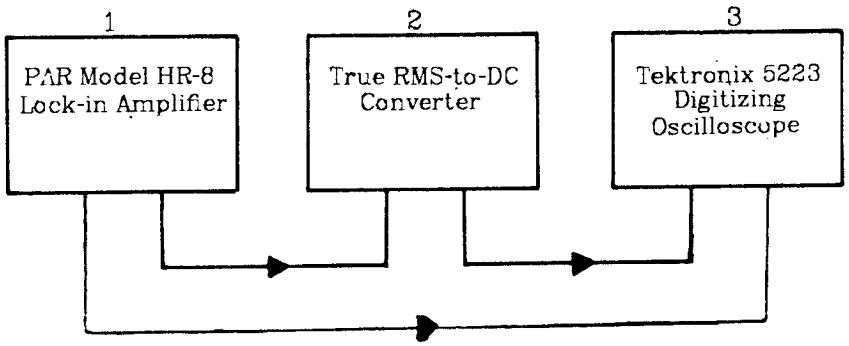

1. Sends sine wave to converter.

2. Converts AC signal to DC level (time constant = 3).

3. Used to determine DC level as compared to ground.

Figure 9: Experimental apparatus for checking conversion factor of rectifier in sine wave experiments.

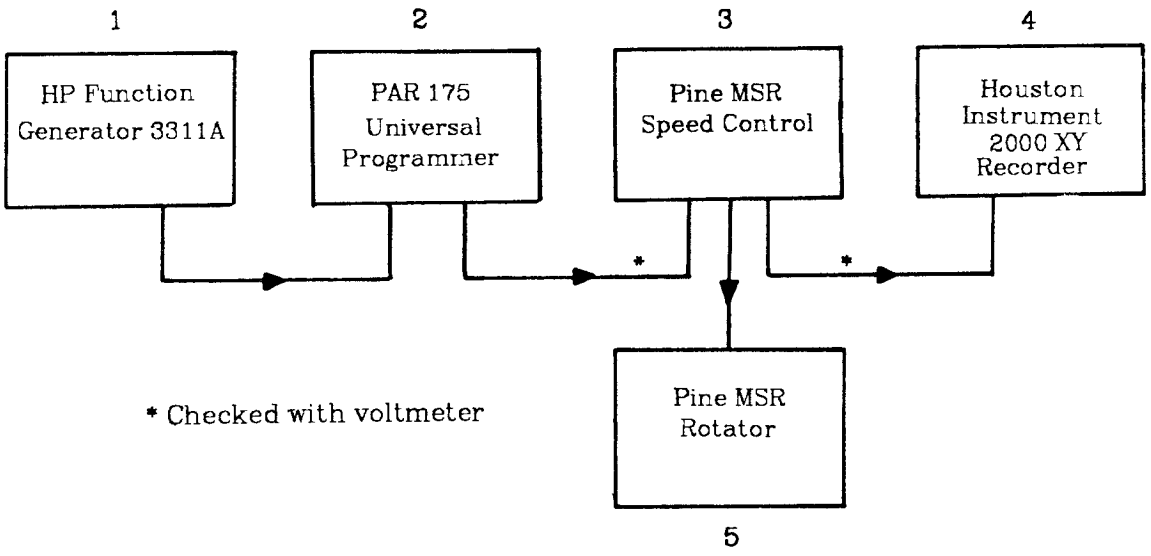

1. Warm up 1-2 hours.
2. Zeros out DC level of HP function generator.
3. Sums voltages (1V = 1000 rpm).
4. Records square wave using time base x-axis.
5. Checked with photo-tachometer.

Figure 10: Initial experimental apparatus for amplitude adjustment of square wave.

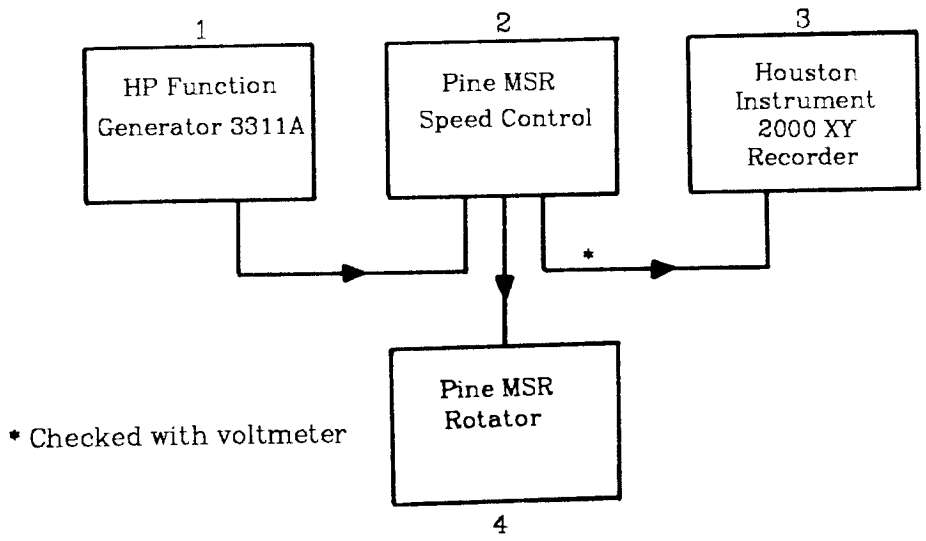

1. Warm up 1-2 hours.
2. Tachometer used to zero out DC level of function generator and set ω.
3. Records square wave using time base x-axis.
4. Checked with photo-tachometer.

Figure 11: Final experimental apparatus for amplitude adjustment of square wave.

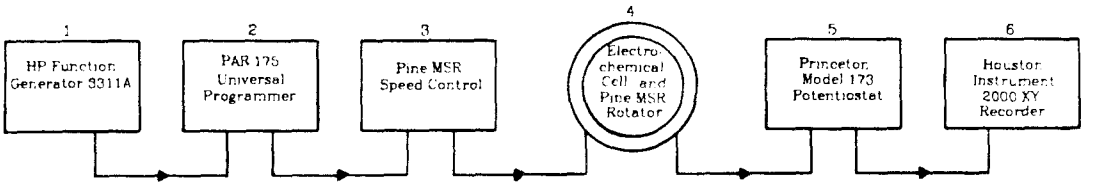

1. Allowed to warm up for 1-2 hours.
2. Used to cancel out DC voltage from HP function generator.
3. Adder: sums potentials from external sources and converts them to rotational velocity (1V = 1000 rpm).
4. Cell and rotator.
5. Constant potential is applied to the cell.
6. Time base x-axis.

Figure 12: Initial experimental apparatus for monitoring current response in square wave experiments.

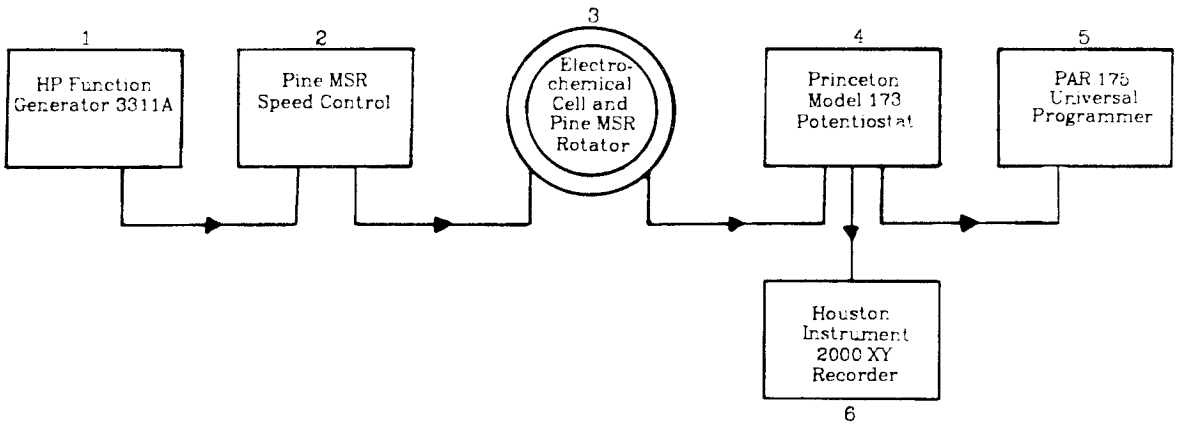

1. Allowed to warm up for 1-2 hours.

2. Adder: sums square wave from HP function generator with set level from the tachometer and converts the voltages to rotational velocity (1V = 1000 rpm).

3. Cell and rotator.

4. Constant potential is applied to the cell.

5. Provides the potential control to the potentiostat.

6. Time base x-axis.

Note: For high frequency data (> 1 Hz.), the currents from the potentiostat were filtered using a low pass, 30 Hz. filter (Rockland Model 432 Dual Hi/Lo Filter) and transferred from a Tektronix 5223 digitizing oscilloscope to the Houston Instrument 2000 XY Recorder.

Figure 13: Final experimental apparatus for monitoring current response in square wave experiments.

4. RESULTS AND DISCUSSION

4.1 Sine wave modulation

In HMRDE experiments involving sinusoidal modulation, the modulated current is recorded as a function of potential. The sine wave component is filtered from the levich current and then converted to a DC signal. Figure 14 contains one example of the i-E and Δi-E curves obtained for a particular experiment. It should be noted that as the potential reaches -0.5 volts, the i-E plot curves up, reflecting background currents while the Δi-E plot remains level. All sine wave experiments were done with the following experimental conditions:

— 1 mM $K_3Fe(CN)_6$;

— $D = 6.84 \times 10^{-6}$ cm^2/sec;

— 0.1 M KCl;

— Pine pyrolytic graphite (area = 0.196 cm^2);

— scan rate = 0.5 V/min;

— time constant = 3 sec;

— Sc = 1600.

While this experimental system is convenient, the experimenter is far-removed from the actual signal and it is difficult to determine the source of any problems. One is unable to decide if deviations from theory are due to equipment failure, solution impurities, or hydrodynamic relaxation failure. With this in mind, several experiments were performed with variation of rotational rate, frequency, and amplitude. Rate of rotation and frequency of modulation were simultaneously varied to test the effect of a constant p factor. All data are

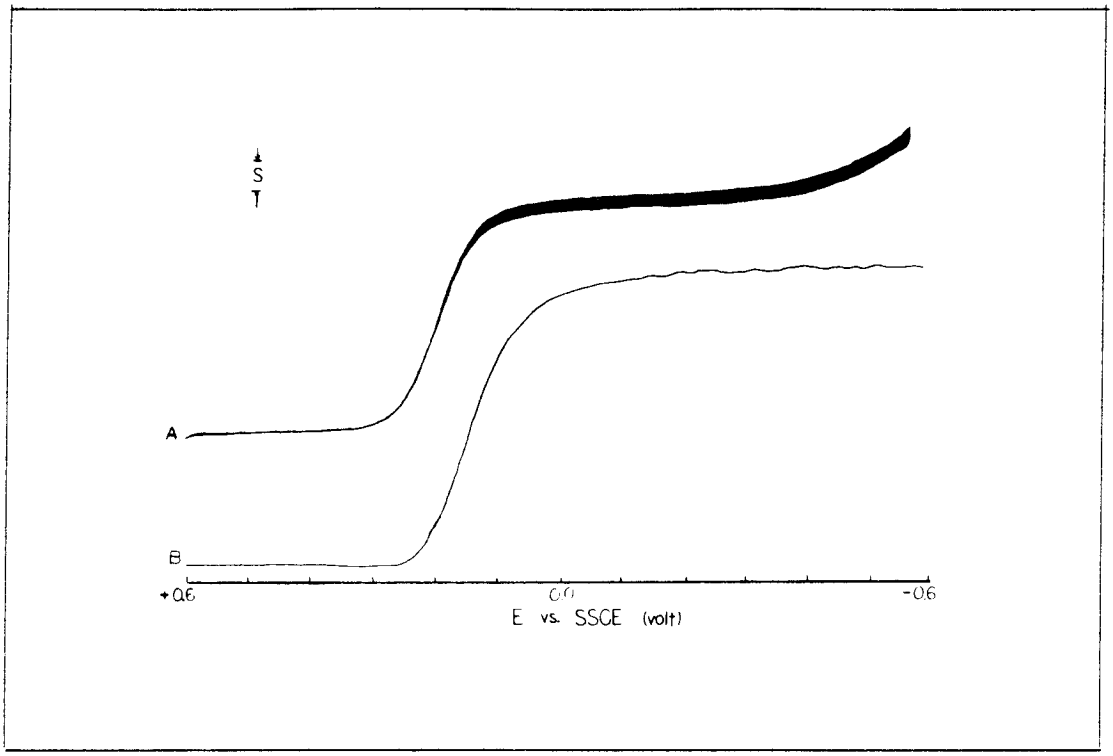

Figure 14: An example of i-E and Δi-E curves for the conditions listed. A) i-E curve, S=50 μA; B) Δi-E curve, S=0.25 μA; ω_0 = 3600 rpm; $\Delta\omega^{1/2}$ = 720 $rpm^{1/2}$; f=6.0 Hz.

displayed in Appendix 2.

Variation of the rotational rate was done for several different frequencies. For each frequency, experimental and theoretical A factors were plotted vs. p factors (figure 15). There is more deviation of the experimental A factors from the theoretical points at low p factors. Since the p factor is a ratio of modulation frequency to rotational rate, it appears that there is more deviation from ideality as the modulation frequency is decreased or the rotational rate is increased. It is difficult to determine whether these differences are due to equipment failure or hydrodynamic relaxation effects. With these limitations in mind, a plot of Δi vs. i_l for each plot was made for each frequency (figure 16). The slope of the plots should be equal to $\Delta\omega^{1/2}/\omega^{1/2}$ and the slopes were

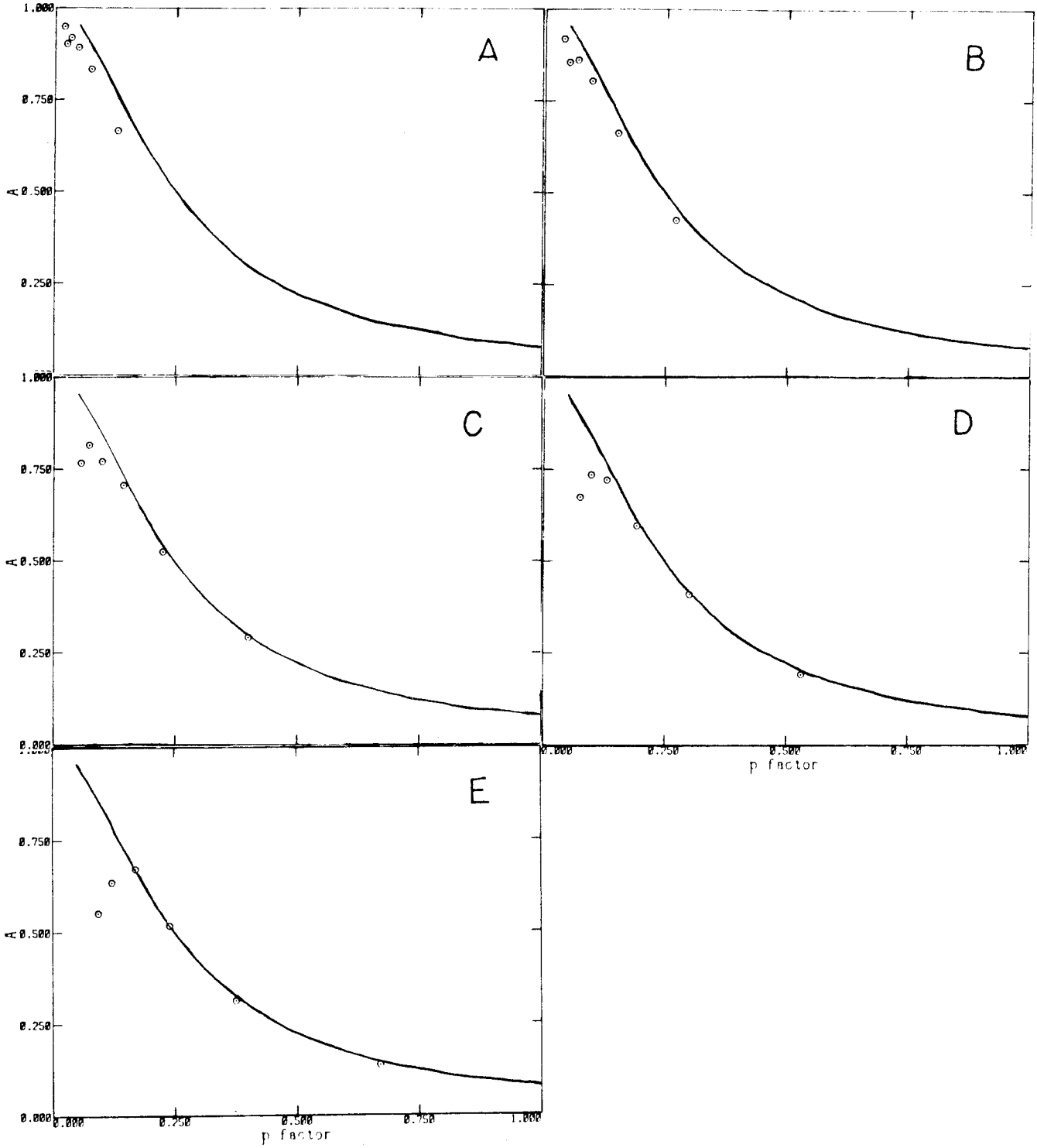

Figure 15: A vs. p factor; rotational rate variation. $\frac{\Delta\omega^{1/2}}{\omega^{1/2}} = 0.10$. Solid lines are theoretical, points are experimental. Frequency = A) 2.0 Hz.; B) 4.0 Hz.; C) 6.0 Hz.; D) 8.0 Hz.; E) 10.0 Hz.

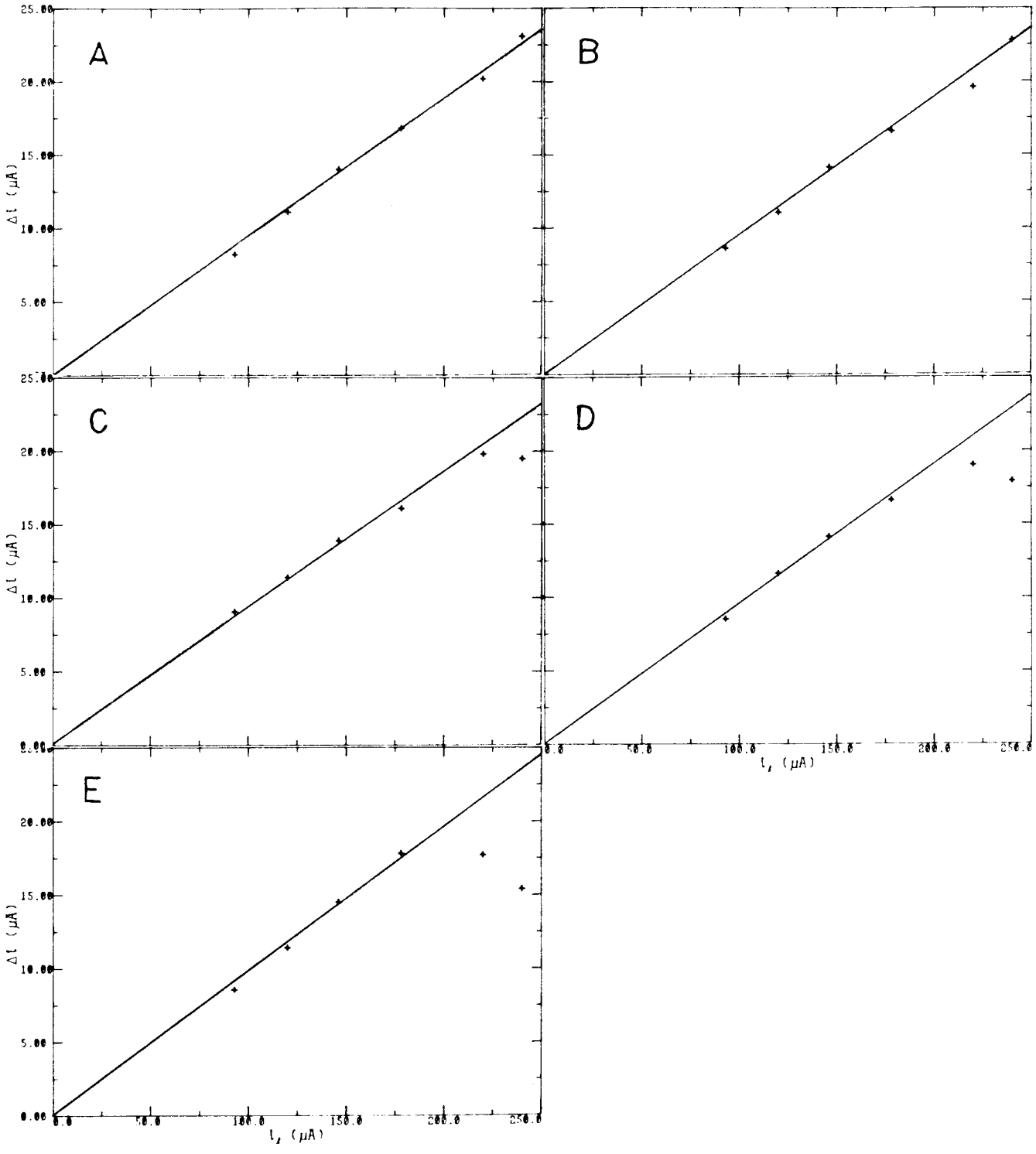

Figure 16: Δi vx. i_1 plots; rotational rate variation. $\frac{\Delta\omega^{1/2}}{\omega^{1/2}} = 0.10$. Points that significantly differed from the theory were not used in calculating the slopes. Frequency:slope = A) 2.0 Hz.:0.092; B) 4.0 Hz.:0.087; C) 6.0 Hz.:0.078; D) 8.0 Hz.:0.088; E) 10.0 Hz.:0.101.

determined using all points except those for which significant deviation was found between theoretical and experimental A factors. The value of $\Delta\omega^{1/2}/\omega^{1/2}$ was set at 0.10 and as shown in figure 16, the experimental slopes are reasonably close to this value.

Rearrangement of the rotational rate data results in a study of frequency variation. Figure 17 consists of six plots of A vs. p factor for a given rotational rate. This perspective shows that experimental A factors follow theory for the lower rotational rates while deviations increase with higher rotational rates. Once again, the cause of the non-ideal behavior is unknown. The modulated current was then plotted vs. the frequency (figure 18). HMRDE theory implies that there should be nc frequency dependence once the A factor is applied and that the Δi vs. f plot should be a horizontal line. Within experimental error this was found to be true for low rates of rotation.

Another series of experiments involved variation of the amplitude of modulation. For a particular rotations rate, frequency of modulation, and thus p factor, the amplitude was set at several values. An A factor was calculated for the experimental data and plotted vs. the p factor (figure 19). Each point represents a unique rotational rate and frequency and 3 or more amplitudes. The data behind these calculations is displayed in Appendix 2 and each value of A has an error of approximately 3%. A fundamental assumption of HMRDE requires that the slope of i_l vs. $\omega^{1/2}$ equal the slope of Δi vs. $\Delta\omega^{1/2}$ plot for a given set of experimental conditions. Figure 20 displays the slopes calculated for the Δi vs. $\Delta\omega^{1/2}$ data. The value of the slope for i_l vs. $\omega^{1/2}$ is 3.0 $\mu A/rpm^{1/2}$ and the results displayed in figure 20 correlate fairly well. These values correspond to a diffusion coefficient of 6.99×10^{-6} cm^2/sec in the RDE case and an average value of 6.07×10^{-6} cm^2/sec for the HMRDE data.

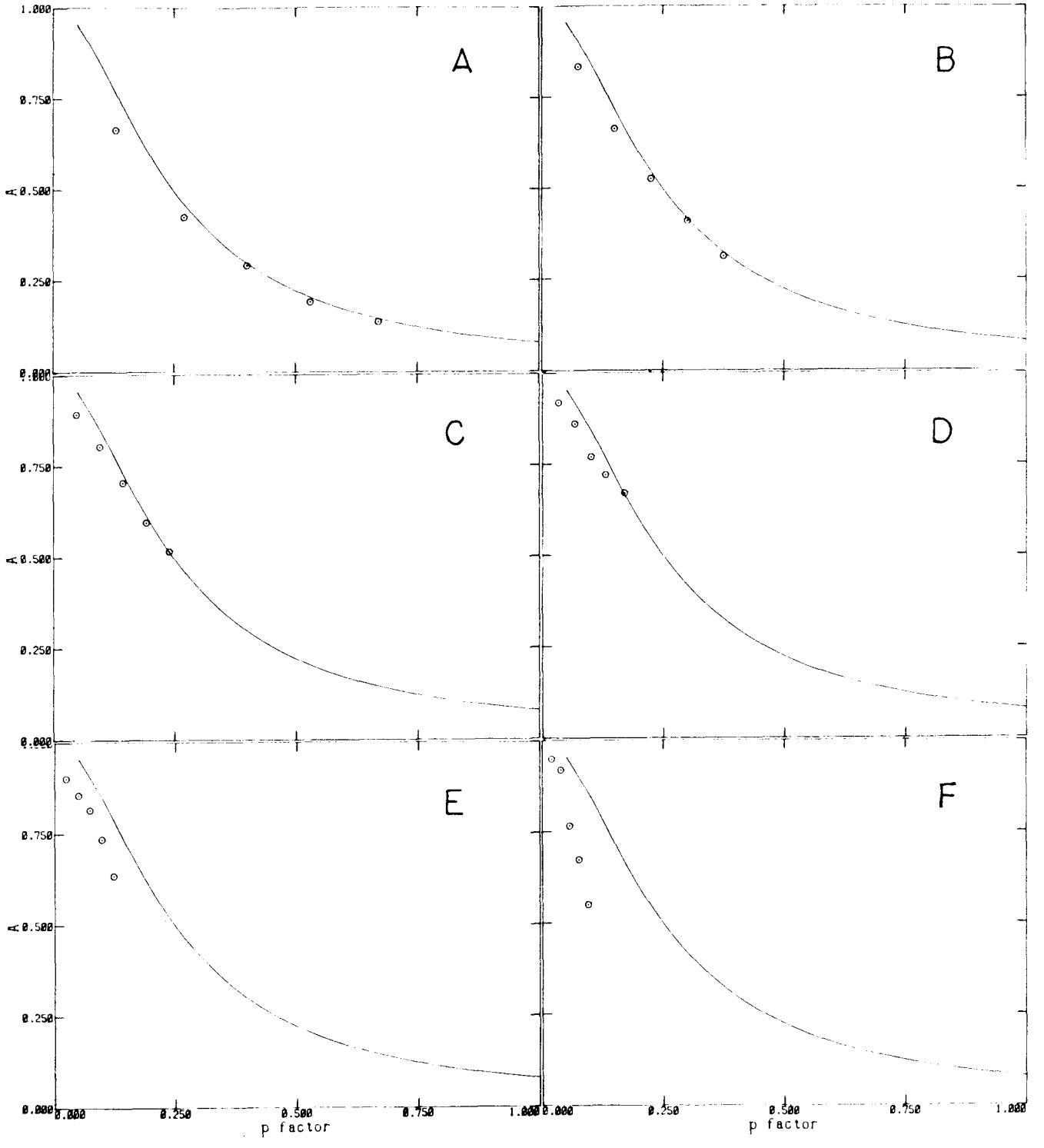

Figure 17: A vs. p factor plots; frequency variation. $\frac{\Delta\omega^{1/2}}{\omega^{1/2}} = 0.10$. Solid lines are theoretical, points are experimental. ω_0 = A) 900 rpm; B) 1600 rpm; C) 2500 rpm; D) 3600 rpm; E) 4900 rpm; F) 6400 rpm.

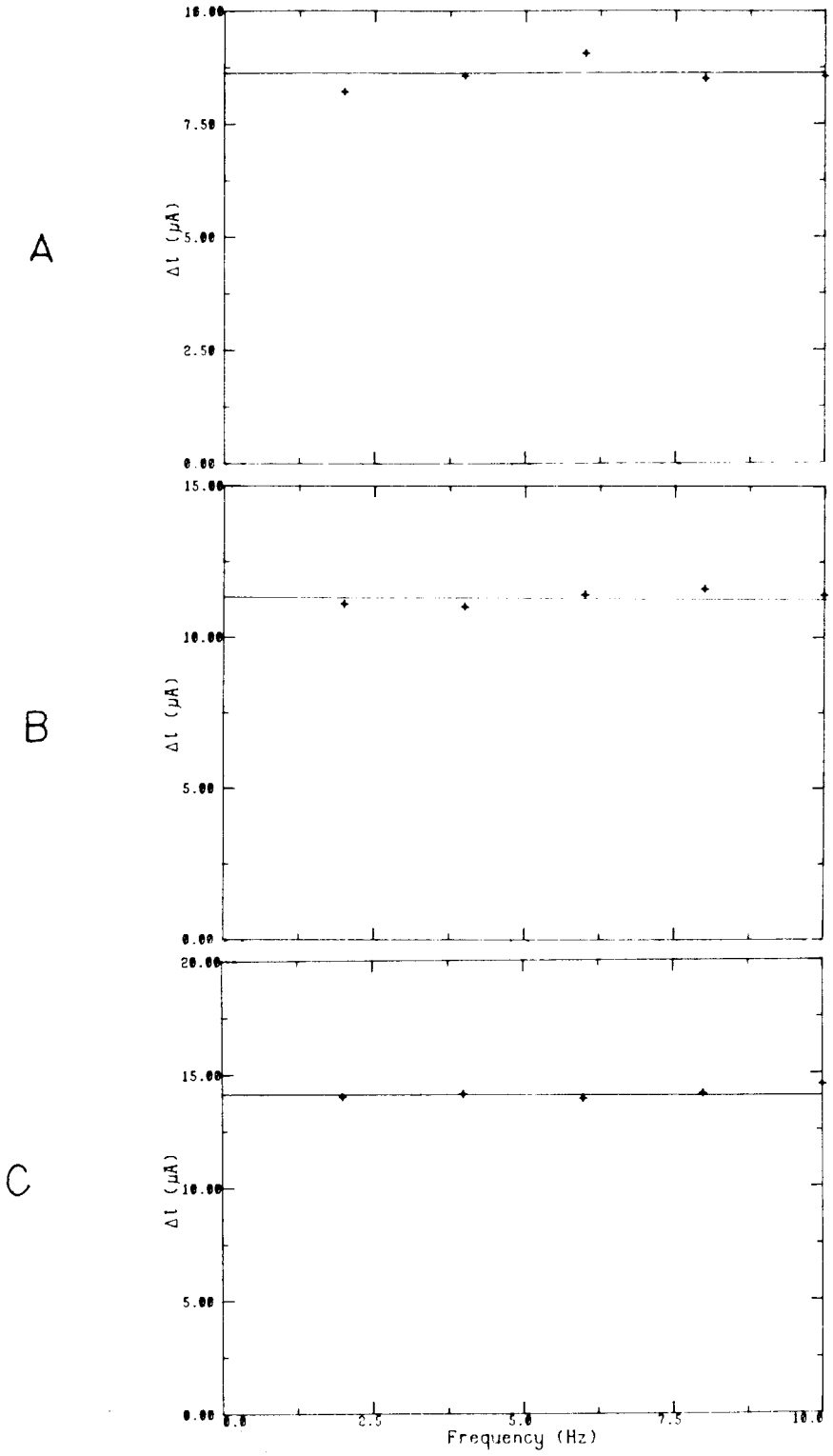

Figure 18: Δi vs. f plots; frequency variation. $\frac{\Delta\omega^{1/2}}{\omega^{1/2}} = 0.10$. A) 900 rpm; B) 1600 rpm; C) 2500 rpm; D) 3600 rpm; E) 4900 rpm; F) 6400 rpm.

D

E

F

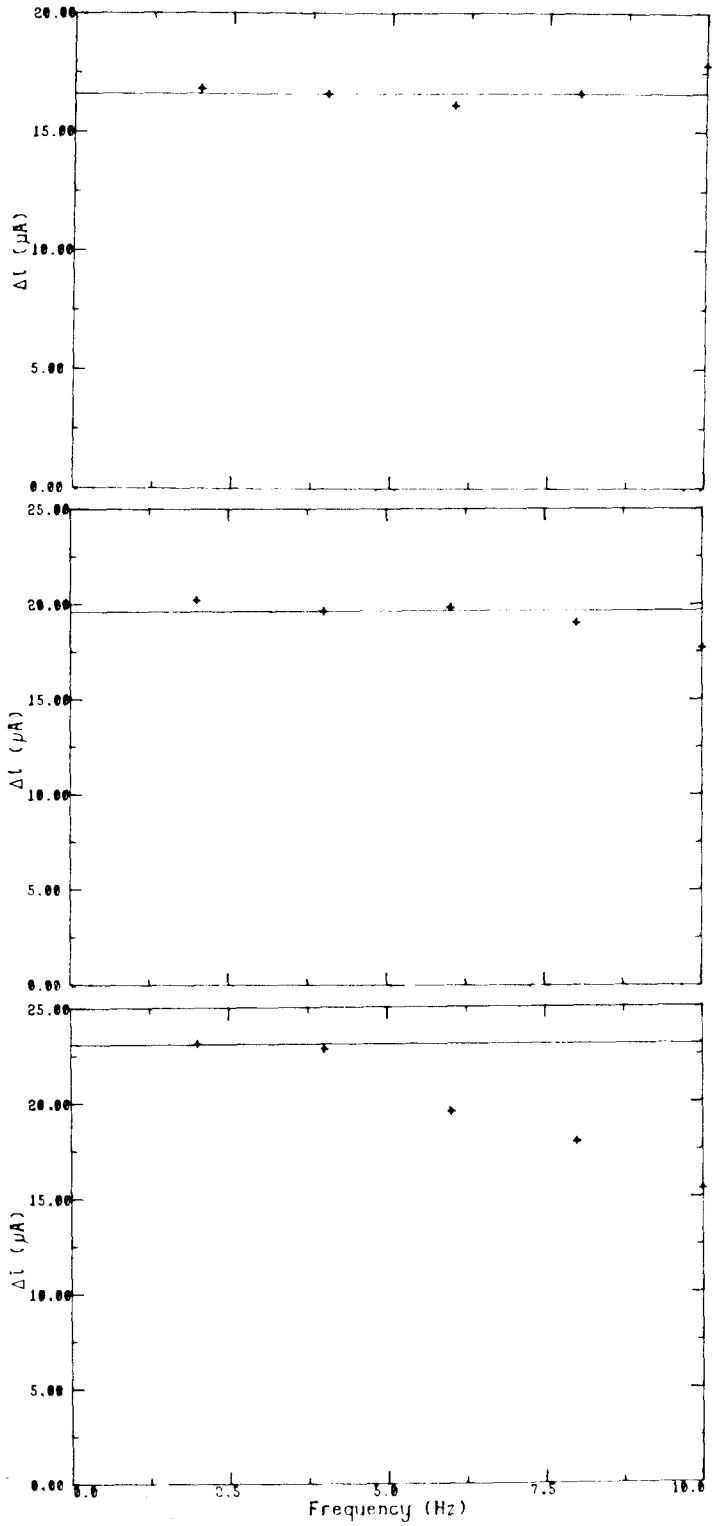

Figure 18: continued.

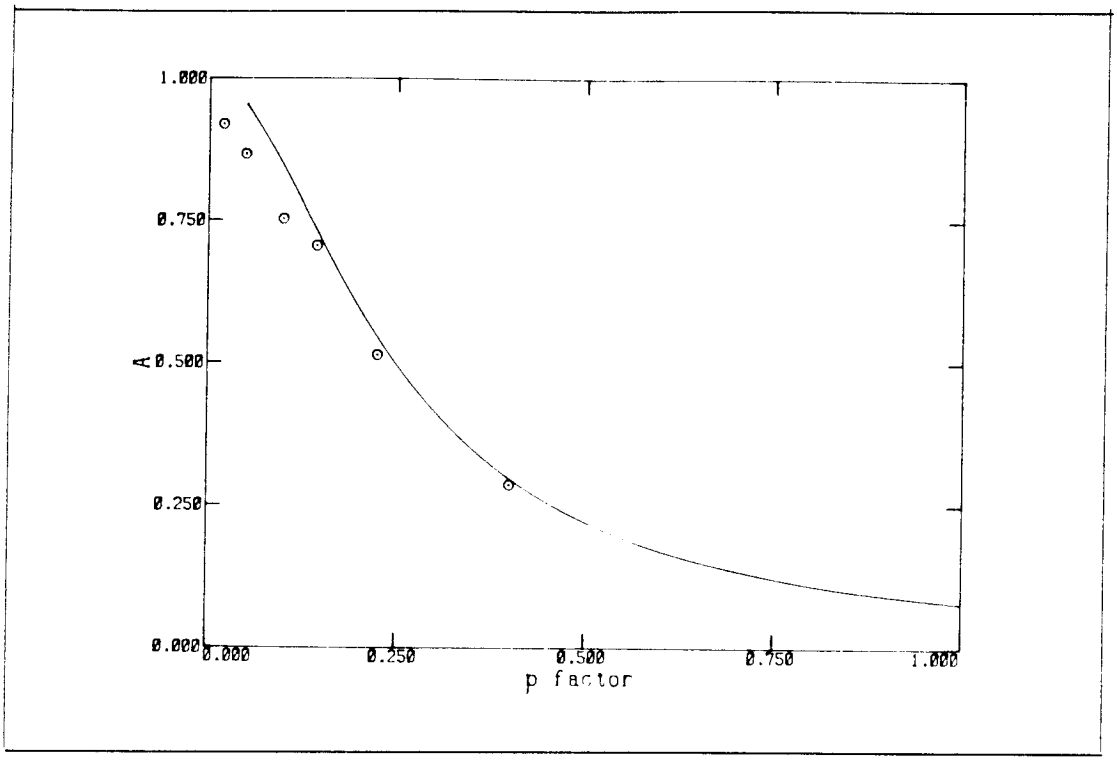

Figure 19: A vs. p factor plot; amplitude variation. Solid lines are theoretical, points are experimental.

Another experiment involved varying both the rotational rate and the frequency in aim of maintaining a constant p factor. For a constant p factor under a given set of experimental conditions, the A factor should remain constant. Figure 21 displays the essential data for this experiment. The experimental A is 0.79 ± 5.3% which differs from the theoretical value of 0.8444. While the values of A are fairly precise considering experimental error, it is difficult to decide to what the deviation from ideality can be attributed.

Finally, the large body of data from the frequency and rotational rate studies was plotted on a single A vs. p factor plot (figure 22). Fair correlation between theoretical and experimental values was achieved. Figure 23 is a similar plot from Tokuda, Bruckenstein, and Miller for other Schmidt numbers and

ω_0 (rpm)	f (Hz)	Slope of Δi vs. $\Delta\omega^{1/2}$ ($\mu A/rpm^{1/2}$)
900	6	2.93
1600	6	2.68
2500	6	2.68
3600	6	2.35
4900	4	2.92
6400	2	2.75

Figure 20: Calculated slopes for Δi vs. $\Delta\omega^{1/2}$ data; amplitude variation.

experimental conditions with much closer correlation.[8] It is difficult to determine the cause of the deviations found in these studies.

ω_0 (rpm)	f (Hz)	A
900	1.5	0.793
1600	2.7	0.790
2500	4.2	0.802
3600	6.0	0.824
4900	8.2	0.826
6400	10.7	0.711

Figure 21: Constant p factor. p factor = 0.1, A = 0.8444.

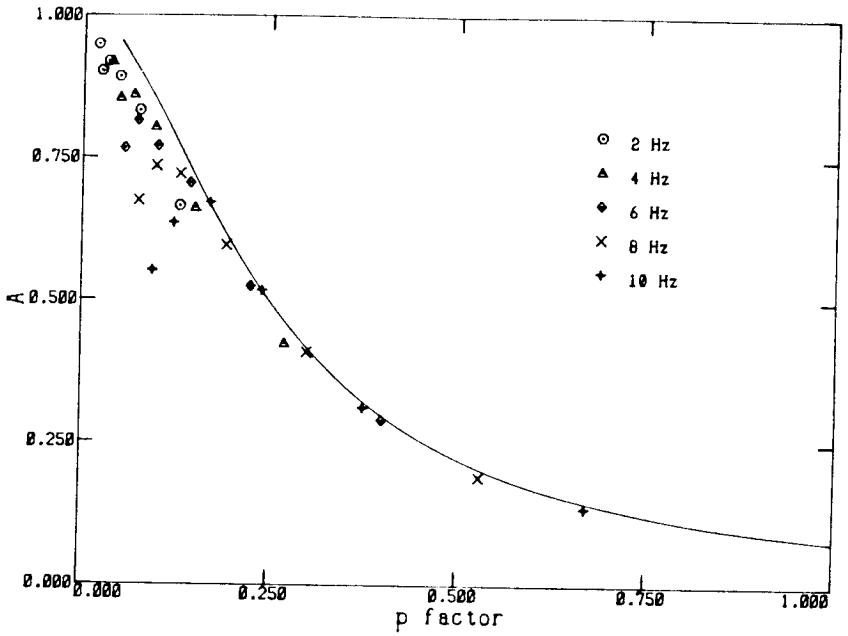

Figure 22: A vs. p factor plot; sine wave modulation. $\Delta\omega^{1/2}/\omega^{1/2} = 0.10$. Solid line is theoretical, points are experimental.

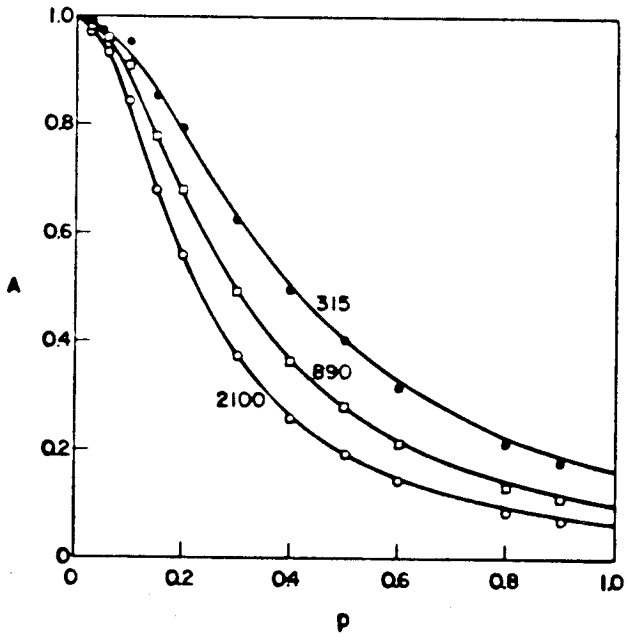

Figure 23: Amplitude factor A as a function of p for Sc values 315, 890, 2100 as marked. Solid lines are theoretical, points are experimental.

4.2 Square wave modulation

Square wave modulation is a simpler process because the modulated current is determined for each given potential. The signal is neither filtered nor rectified and Δi is directly recorded. Therefore, when deviations occur, the causes are more obvious. Appendix 3 contains the data for all square wave experiments. It is important to note that the Δi's are derived from these relationships.

$$\Delta i_{experimental} = \text{raw data}$$

$$\Delta i_{calculated} = i_l \frac{\Delta \omega^{1/2}}{\omega^{1/2}}$$

All square wave experiments are done under the following conditions:

— 1 mM $K_3Fe(CN)_6$;

— $D = 6.84 \times 10^{-6}$ cm^2/sec;

— 0.1 M KCl;

— Pine pyrolytic graphite (area = 0.196 cm^2);

— potential = -0.1 volts;

— Sc = 1600.

The rate of rotation was varied in one experiment. For this experiment, a linear levich plot (μA vs. $rpm^{1/2}$) was found with a corresponding slope of 2.97 $\mu A/rpm^{1/2}$ (figure 24). This compares with a value of 2.96 $\mu A/rpm^2$ for the plot of Δi vs. $\Delta \omega^{1/2}$ (figure 25). In this case, an excellent correlation between theory and experiment was found. The data was then plotted as Δi vs. i_l (figure 26) with similar agreement.

The frequency of modulation studies were done for 900 rpm and 2500 rpm. An A factor vs. frequency plot shows that the modulated current decreases with increasing frequency (figure 27). This decrease is dramatically shown in the comparison of motor response to current response of figure 28. For the low frequencies ($\leq$ 1 Hz) the motor response is a perfect square wave. At frequencies greater than 1 Hz, the motor has increasing difficulties following the square wave. Deviations from ideality occur much sooner (0.5 Hz) for current response as evidenced by rounding of the waves. The degree of the rounding increases until a straight line current response is obtained at 10 Hz. This inability to approach hydrodynamic steady state is shown in the Δi vs. p factor plot for this data (figure 29). At low p factor or frequency, the experimental points follow theory while significant deviations are found at the other end of the spectrum.

Finally, a study of amplitude variation was completed for square wave modulation. A plot of Δi vs. $\Delta\omega^{1/2}$ was done for the data (figure 30). The experimental points deviate from the calculated values more as one reaches higher amplitudes. Within experimental error, the slope of the lines through the experimental data and calculated data correlate well. The plot of Δi vs. $\Delta\omega^{1/2}$ reflects a diffusion coefficient of 6.84×10^{-6} $cm^{1/2}/sec$.

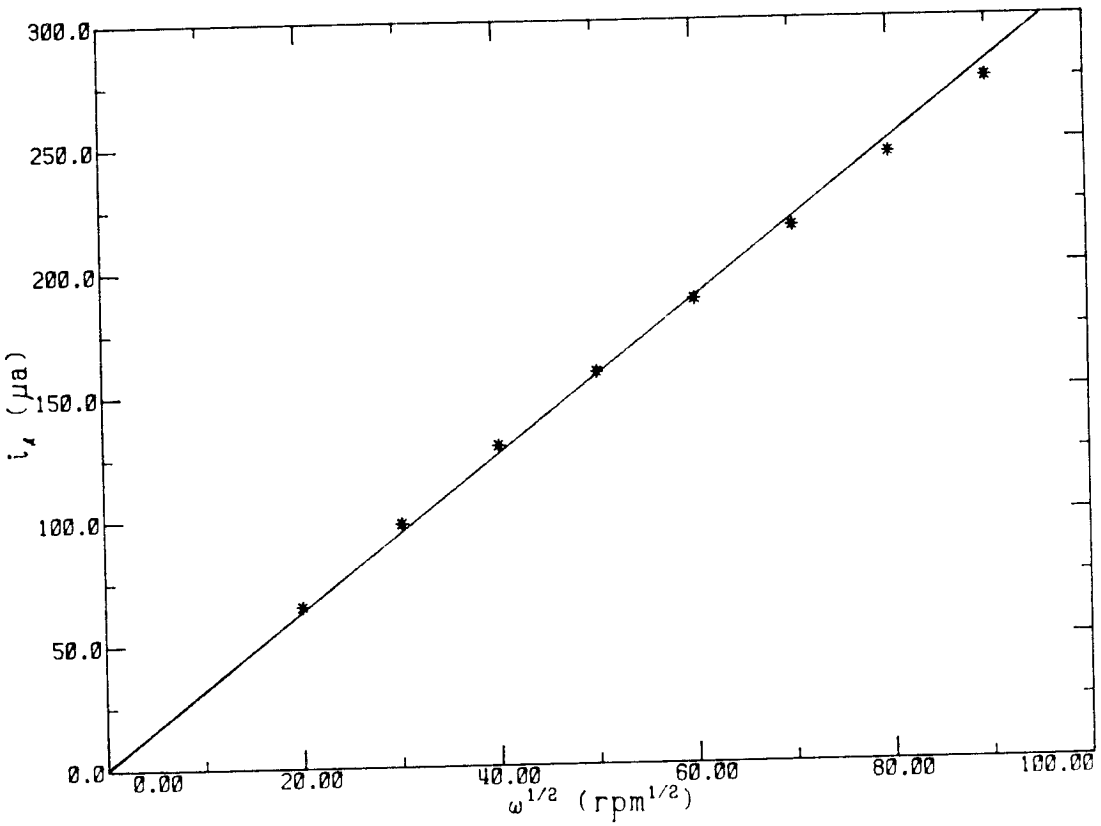

Figure 24: Levich plot.

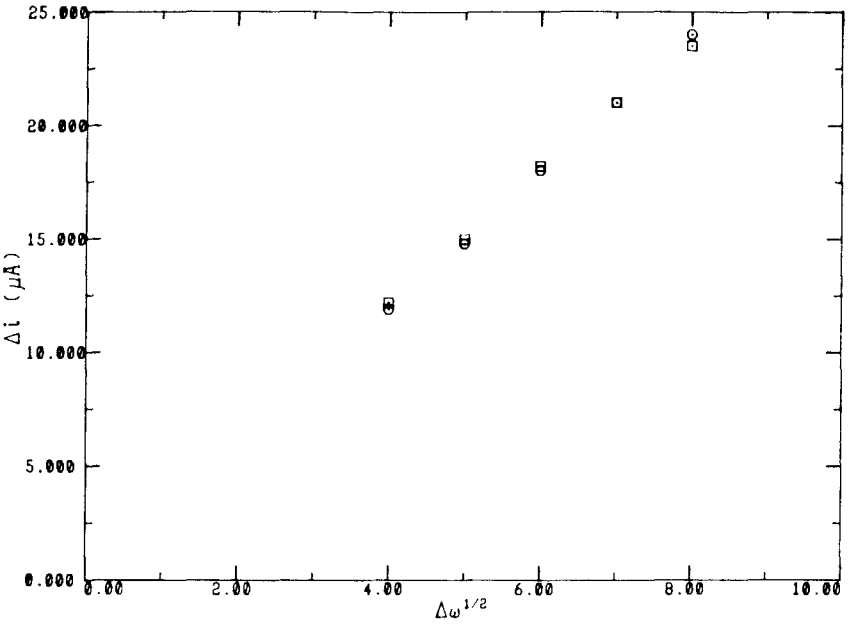

Figure 25: Δi vs. $\Delta\omega^{1/2}$ plot; rotational rate variation. $\frac{\Delta\omega^{1/2}}{\omega^{1/2}} = 0.10$; f=0.10 Hz.; ⊙ = calculated, ⊡ = experimental.

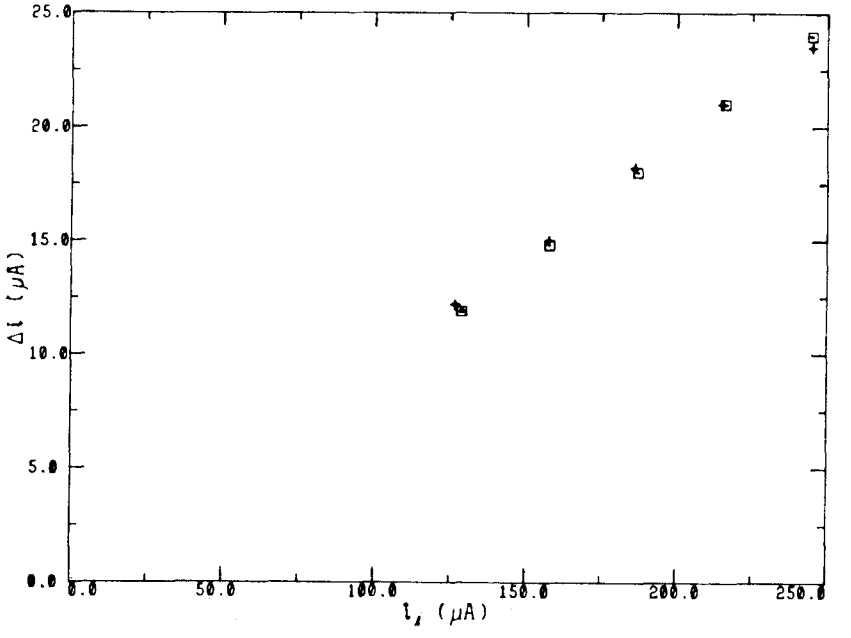

Figure 26: Δi vs. i_j plot; rotational rate variation. $\frac{\Delta\omega^{1/2}}{\omega^{1/2}} = 0.10$; f=0.10 Hz.; ⊡ = calculated, ✦ = experimental. Calculated slope = 0.100; experimental slope = 0.101.

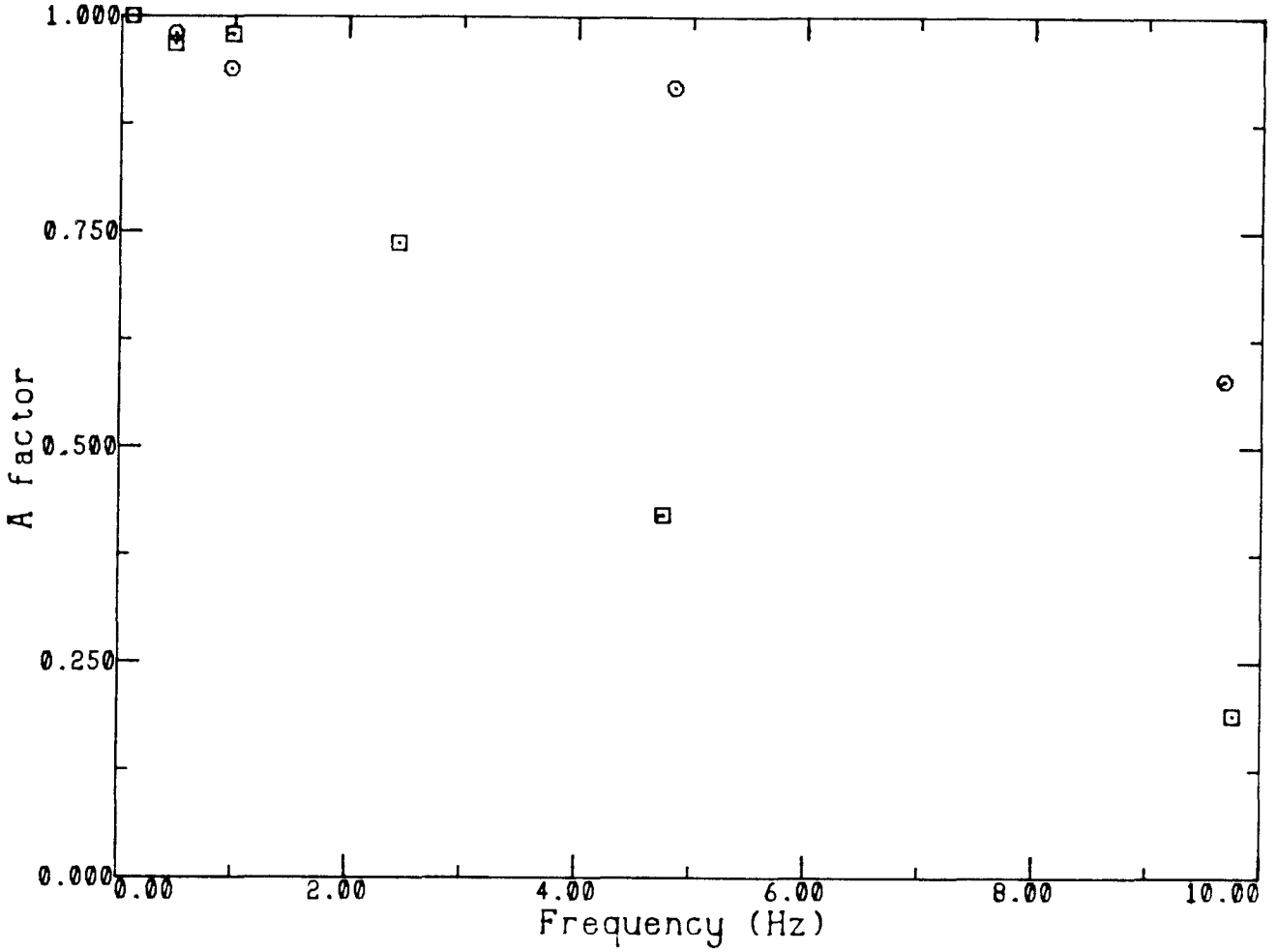

Figure 27: A factor vs. frequency plot; frequency variation. $\frac{\Delta\omega^{1/2}}{\omega^{1/2}} = 0.10$.
⊡ = 900 rpm, ⊙ = 2500 rpm.

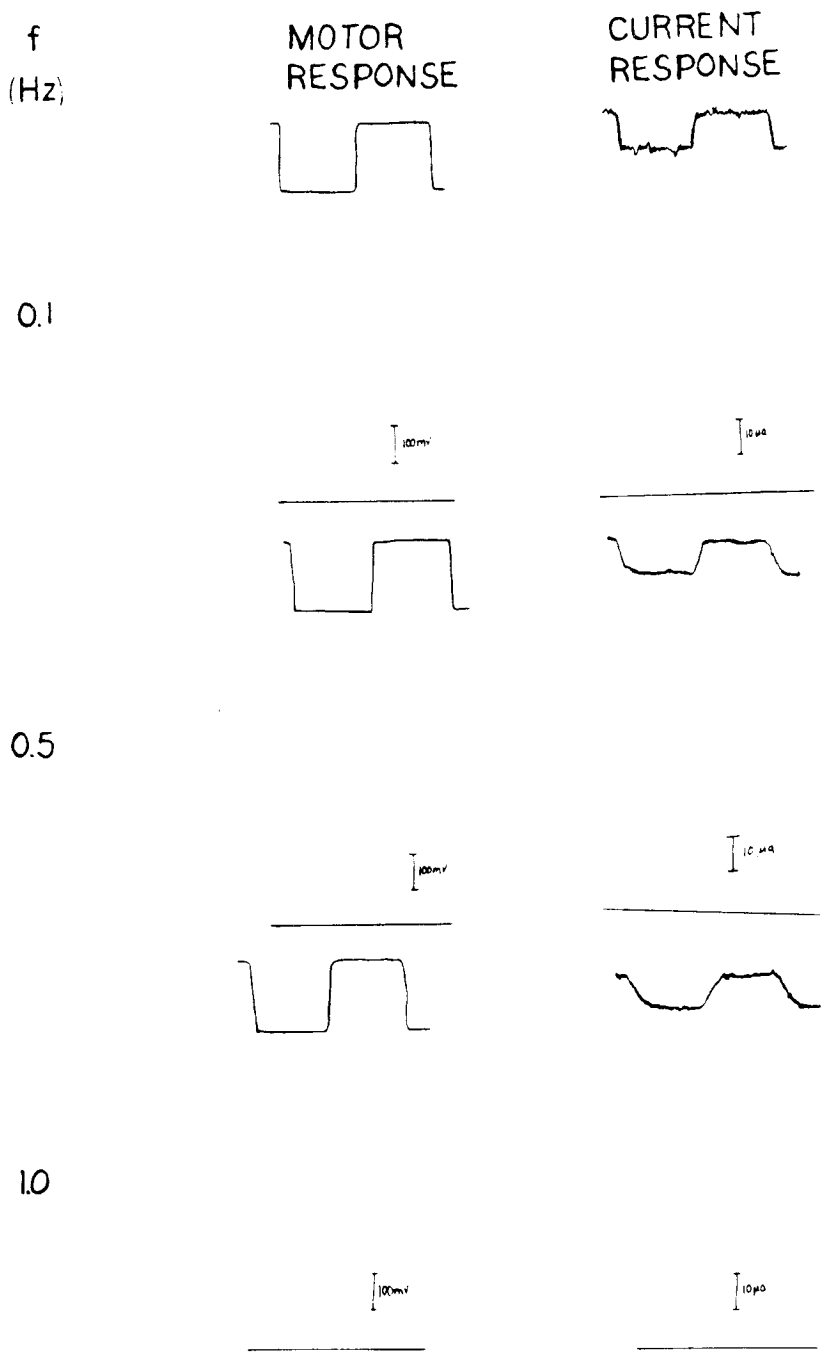

Figure 28: Comparison of current response to motor response for ω_0 = 900 rpm. $\Delta\omega^{1/2}$ = 180 rpm$^{1/2}$; $\frac{\Delta\omega^{1/2}}{\omega^{1/2}}$ = 0.10.

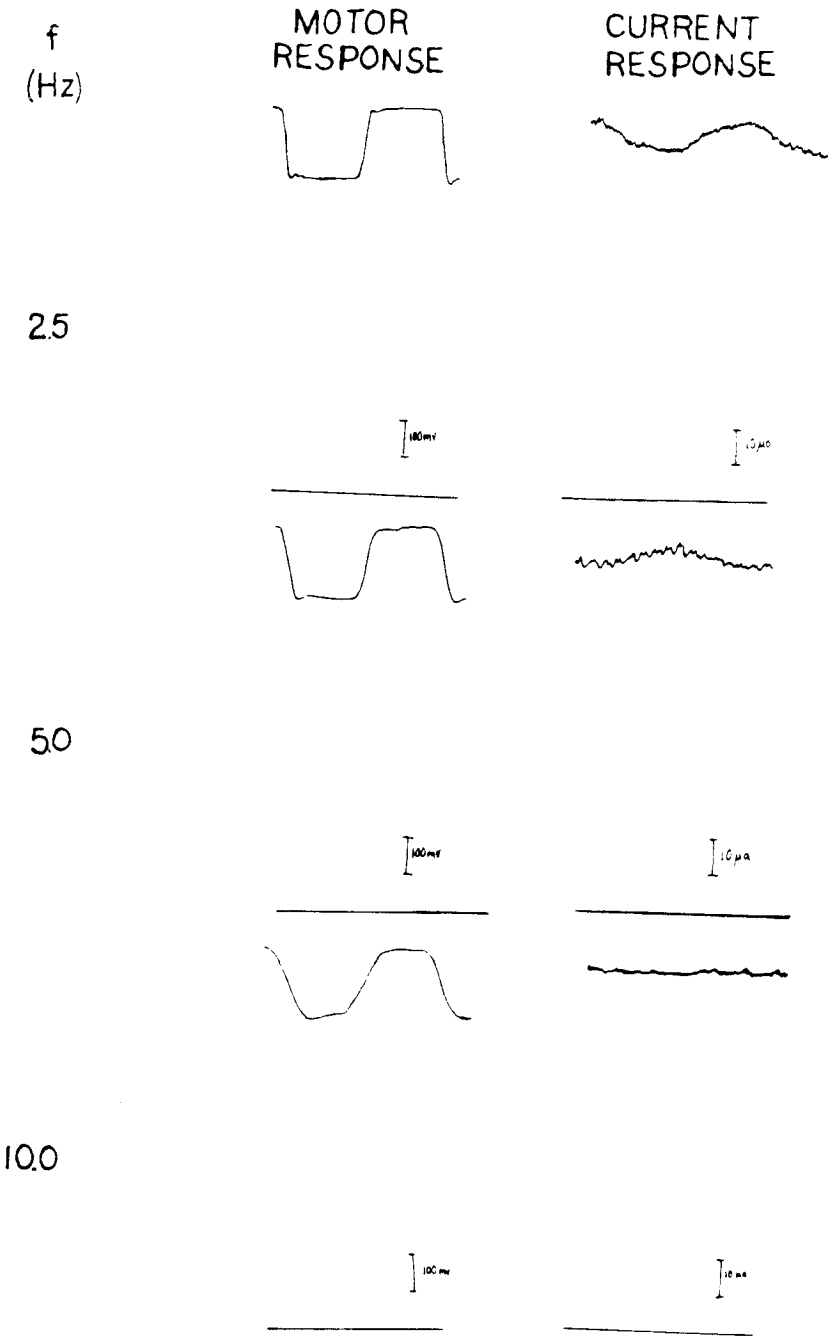

Figure 28: continued.

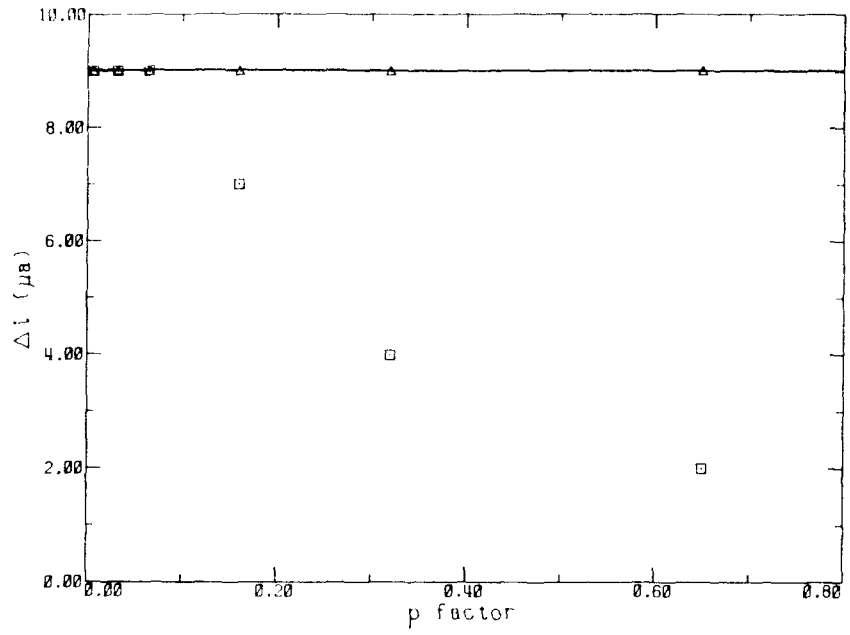

Figure 29: Δi vs. p factor plot; frequency variation. ω_0 = 900 rpm. $\frac{\Delta\omega^{1/2}}{\omega^{1/2}}$ = 0.10. △ = calculated, ⊡ = experimental.

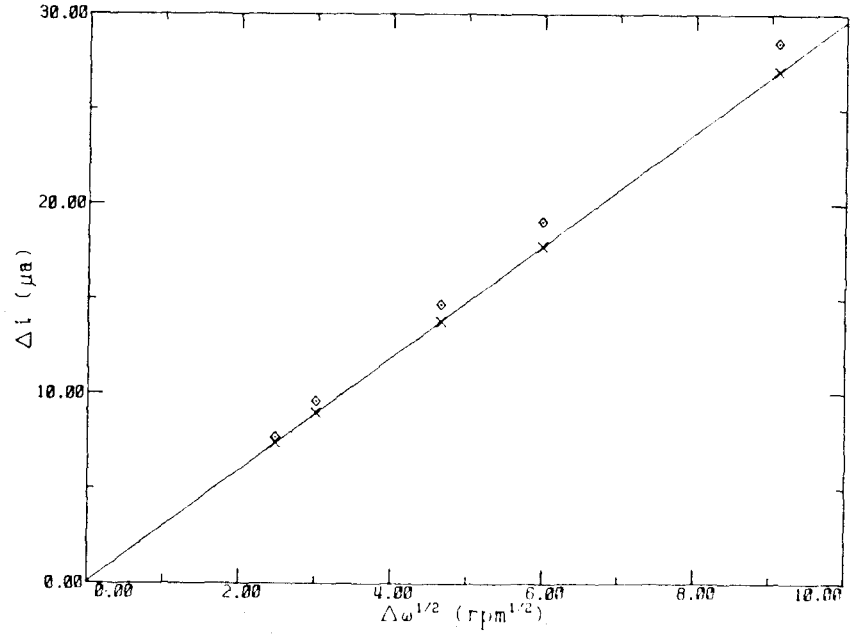

Figure 30: Δi vs. $\Delta\omega^{1/2}$ plot; amplitude variation. ω_0 = 900 rpm; f=0.10 Hz.; p factor = 0.0065; × = calculated, ◇ = experimental. Experimental slope = 3.13 $\mu A/rpm^{1/2}$; calculated slope = 2.97 $\mu A/rpm^{1/2}$.

4.3 Poly(4-vinylpyridine) Experiments

Successive cyclic voltammograms for the reduction of $Fe(CN)_6^{3-}$ at a graphite electrode coated with PVP were recorded. The response was comparable to that reported by Shigehara, Oyama, and Anson.[17] However, once the PVP-coated electrode was transferred to a pure supporting electrolyte, the magnitude of the current was unaffected by repeated cycling for only 15 minutes. Within 1.5 hours, the magnitude had been halved. Since a constant response could not be achieved, it was decided to study Nafion-coated electrodes.

4.4 Nafion-coated electrodes

Reproducible, steady response from the $Ru(NH_3)_6^{3+/2+}$ couple in the Nafion coatings were obtained when loaded in relatively concentrated solutions of $Ru(NH_3)_6^{3+}$ before transferring them to less concentrated solutions of $Ru(NH_3)_6^{3+}$ as suggested by Liu and Anson.[18] Figure 31 shows the bare electrode response compared to that of the Nafion coated electrode for the $Ru(NH_3)_6^{3+/2+}$ couple. All experiments were done in 0.1 M $Ru(NH_3)_6Cl_3$, 0.2 M CH_3COONa at pH 5.5 at a BPG electrode (Ar=0.174 cm^2). The formal potential of the $Ru(NH_3)_6^{3+/2+}$ couple incorporated in a Nafion coating is 100 mv negative of that for the same couple in homogeneous solution. This shift is similar to that reported and analyzed by Tsou and Anson.[19]

The technique of non-steady state RDE was used for Nafion coated electrodes as described in the experimental section. Figure 32 shows the bare electrode i-E curves for each scan rate and the rotational rate for which a steady-state response was obtained. These matched scan rate and rotational rates were used on a Nafion coated electrode (figure 33). The polymer coated electrodes were also scanned at 1 mv/sec at each rotational rate. The difference in these two i-E curves were taken and compared to the response of the Nafion coated electrode in pure supporting electrolyte, shown in figure 34. While the

calculated response is similar to the response in pure supporting electrolyte, in this case it has not been shown to be true for other polymer systems.

Square wave experiments were performed on the Nafion coated electrodes. The modulated current obtained experimentally was larger than that predicted from the theory of HMRDE. The cause of this discrepancy was not discovered.

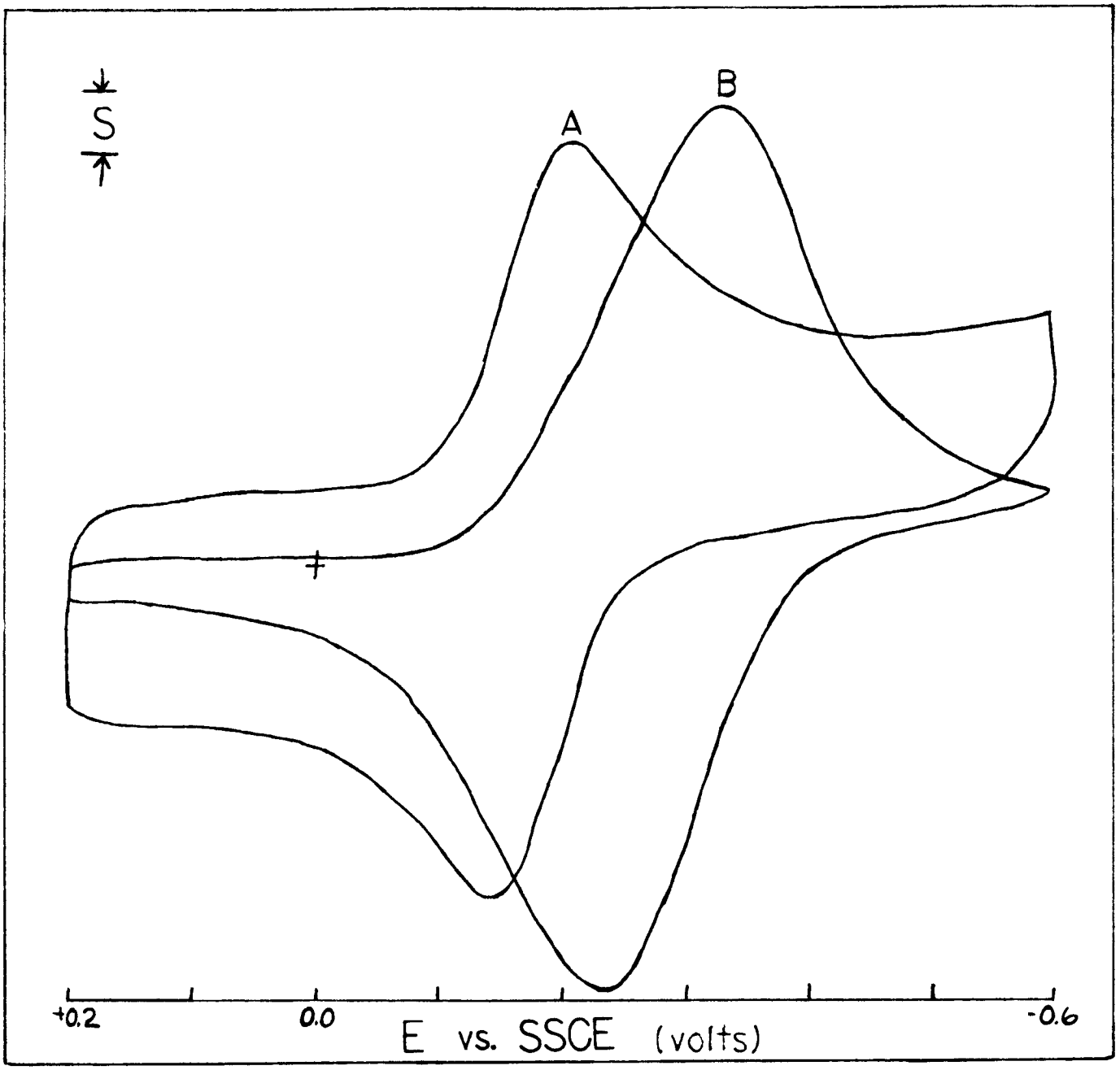

Figure 31: Cyclic voltammograms for comparing bare electrode response to Nafion-coated response for the $Ru(NH_3)_6^{3+/2+}$ couple. Scan rate = 200 mv/sec. A) Bare BPG electrode response, S=1.0 μA; B) Nafion-coated electrode response, S=10.0 μA.

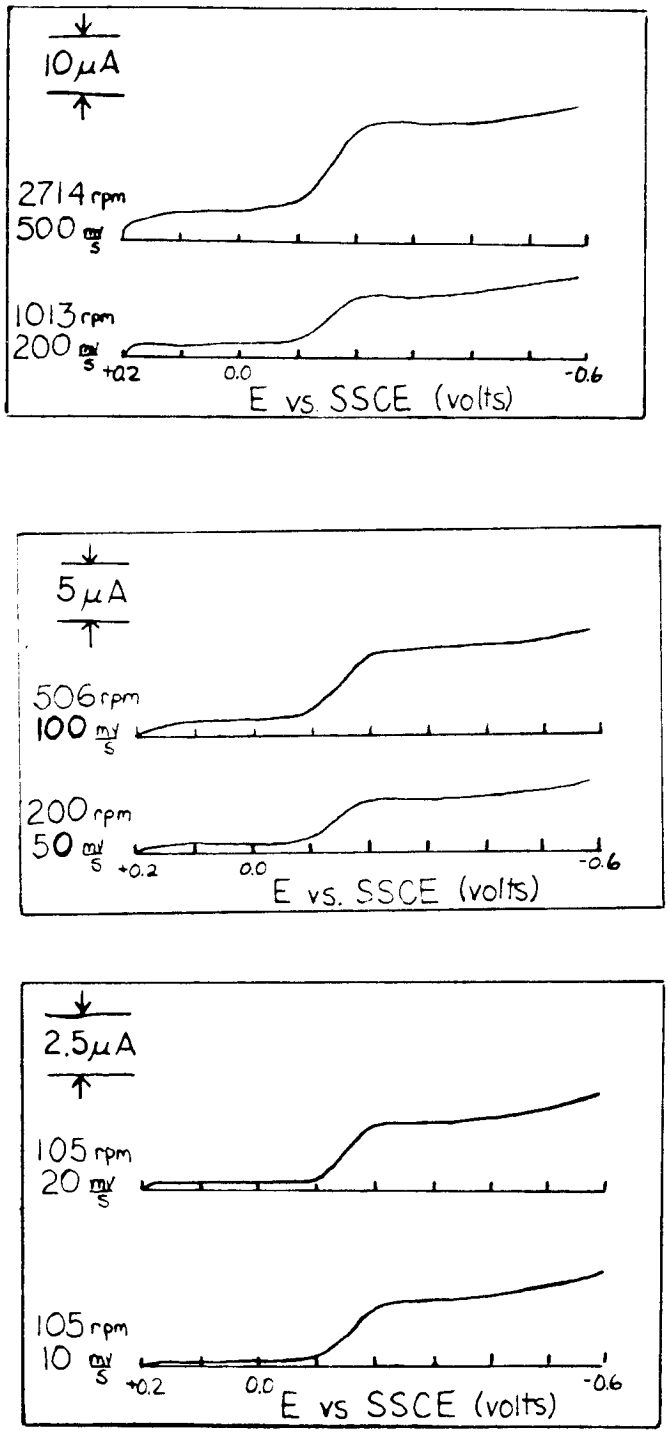

Figure 32: Matching of ω_0 and scan rate to obtain steady-state response for bare electrode.

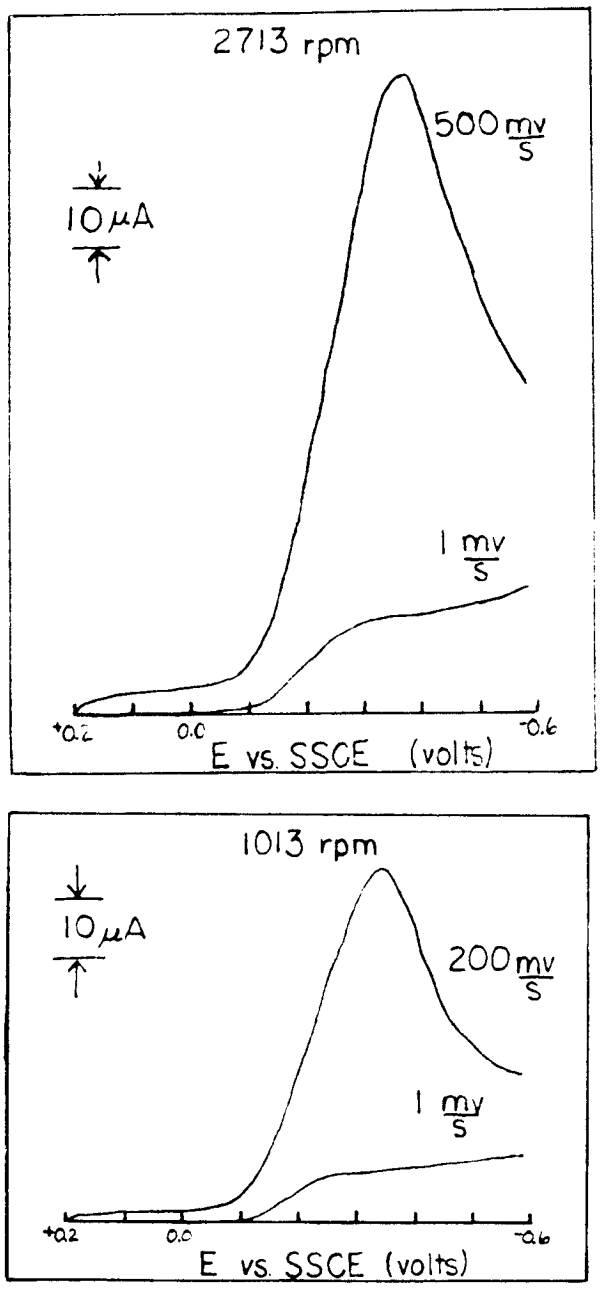

Figure 33: Matching of ω_0 and scan rate to obtain steady-state response for Nafion-coated electrode. 2 μl of 0.5% Nafion, $\Gamma = 4.1 \times 10^{-9}$ moles/cm^2.

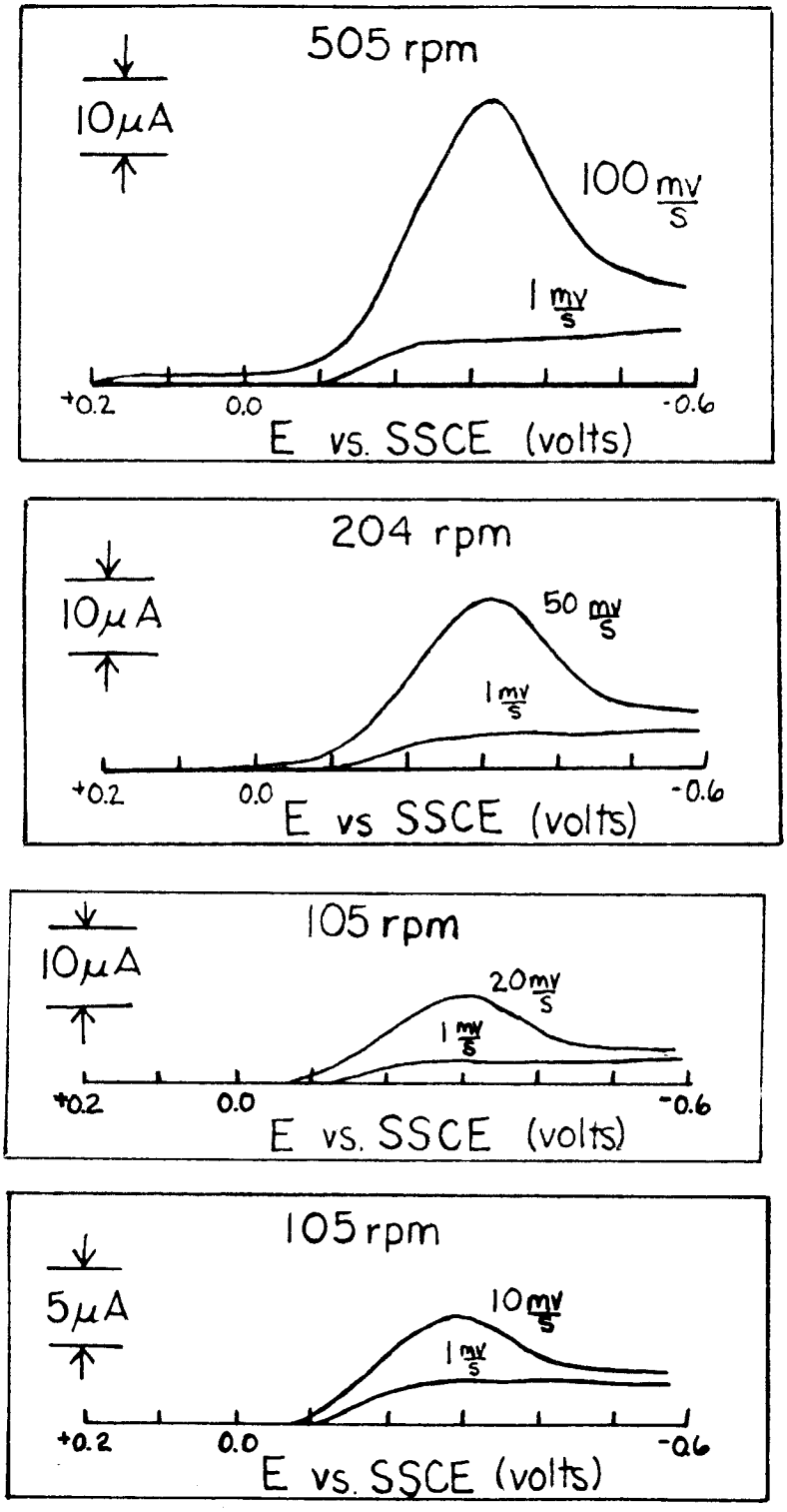

Figure 33: continued.

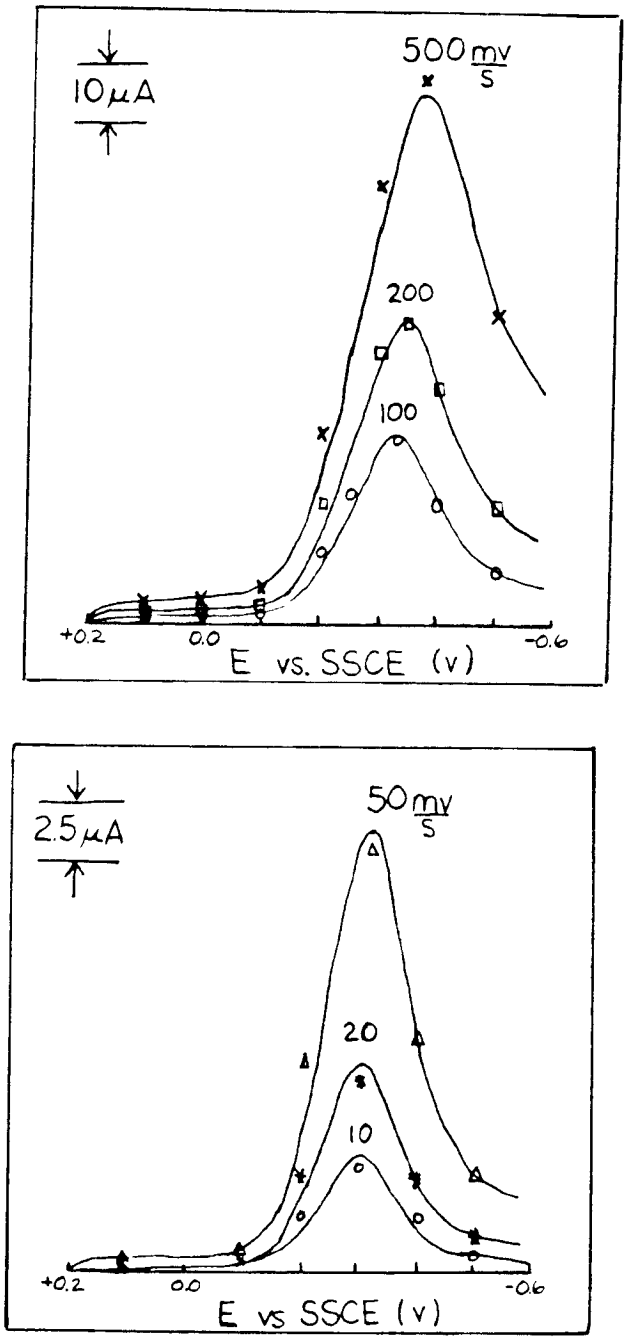

Figure 34: Solid lines are current response in pure supporting electrolyte, points are the difference between the 2 curves in figure 33 for each scan rate and rotation rate.

4.5 Iron(III) meso-tetraphenylporphine

It was decided to use the non-steady RDE on the catalyzed reduction of oxygen by FeTPP adsorbed on graphite electrodes. As shown in figure 35, catalysis of oxygen reduction was found. The catalysis discovered was less in magnitude and lacked the prewave reported by Shigehara and Anson (figure 36).[20] One of the problems encountered in this work was that electrodes prepared in a similar manner produce different amounts of catalysis. Figure 37 displays a different response for the catalysis of oxygen reduction under the same conditions as figure 35. In addition, successive scans show excessive losses in catalytic activity (figure 38). Non-steady state RDE requires the use of a steady, reproducible system. Because of the difficulties with stability, this study of FeTPP was abandoned.

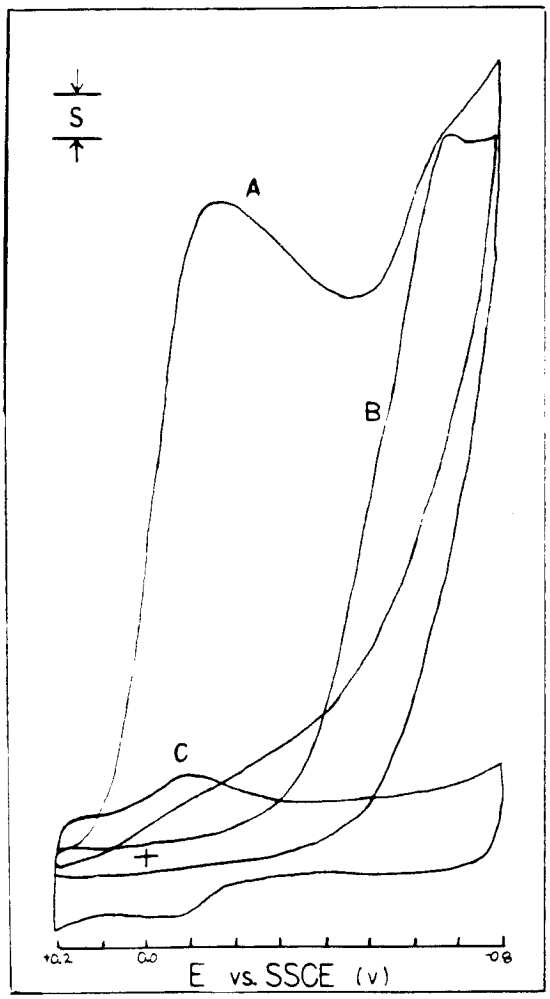

Figure 35: Cyclic voltammogram for oxygen reduction by FeTPP. 0.1 M $HClO_4$ + 0.1 M $NaClO_4$. A) FeTPP coated electrode; O_2 saturated solution; S=10 μA; B) Bare BPG; O_2 saturated solution; S=10 μA; C) FeTPP coated electrode; no O_2; S=1 μA. $\Gamma = 10^{-9}$ moles/cm^2.

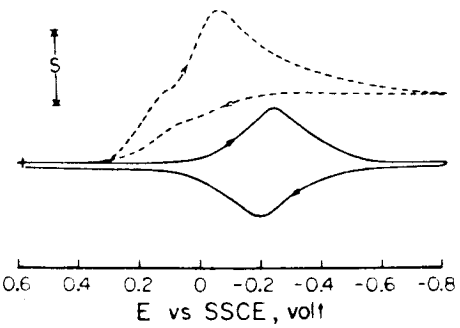

Figure 36: Cyclic voltammograms for adsorbed FeTPP in the absence (solid curves, S=5 μA) and in the presence (dashed curves, S=25 μA) of O_2 (saturated). The pyrolytic graphite electrode (Ar = 0.17 cm^2) was coated wih 6 x 10^{-8} moles/cm^2 or FeTPP. Supporting electrolyte: 0.1 M $HClO_4$ + 0.1 M $NaClO_4$; scan rate = 20 mv/sec. [20]

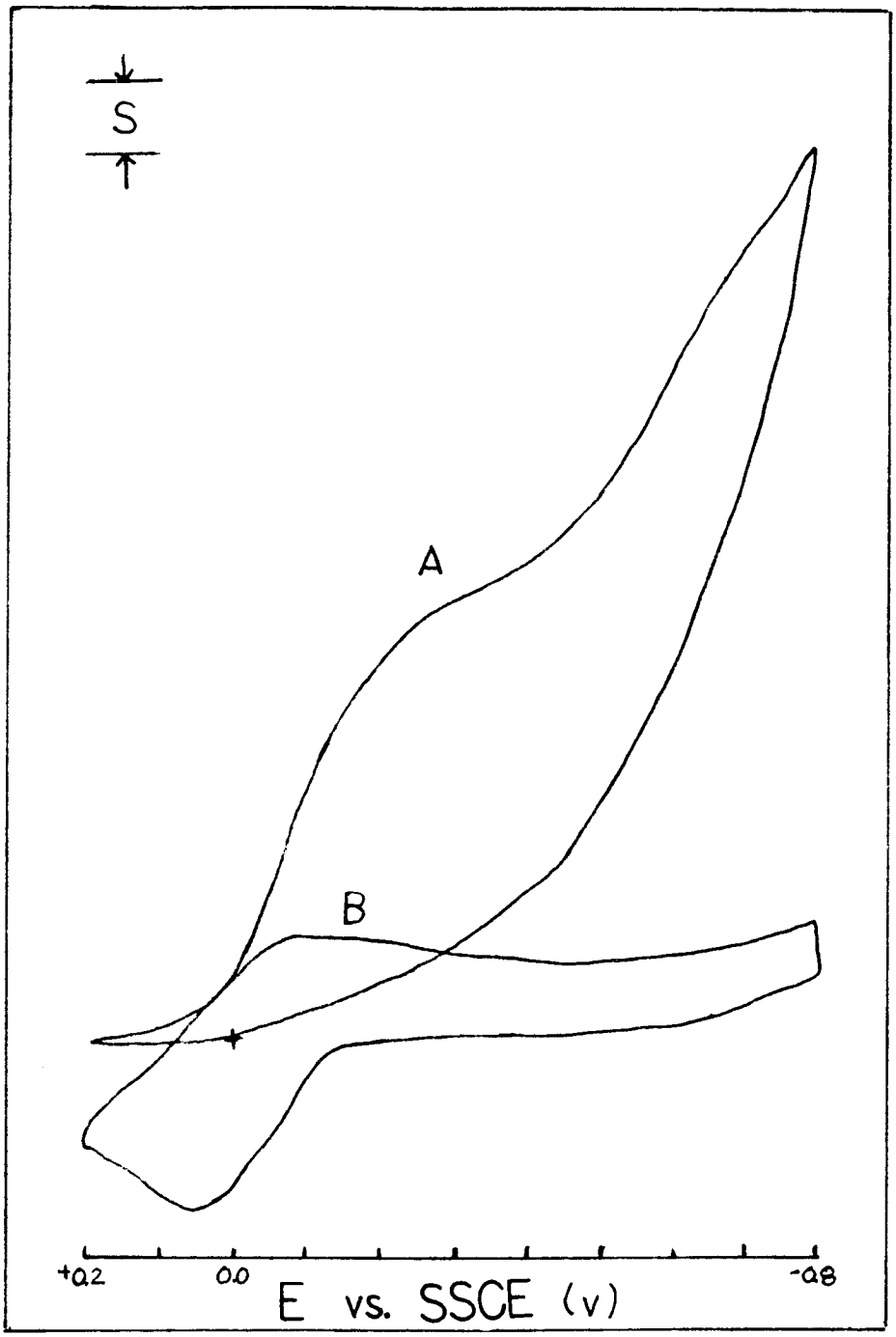

Figure 37: Cyclic voltammogram for O_2 reduction by FeTPP. A) O_2 saturated solution, S=10 μA; B) no O_2, S=1.0 μA. 0.1 M $HClO_4$ + 0.1 M $NaClO_4$

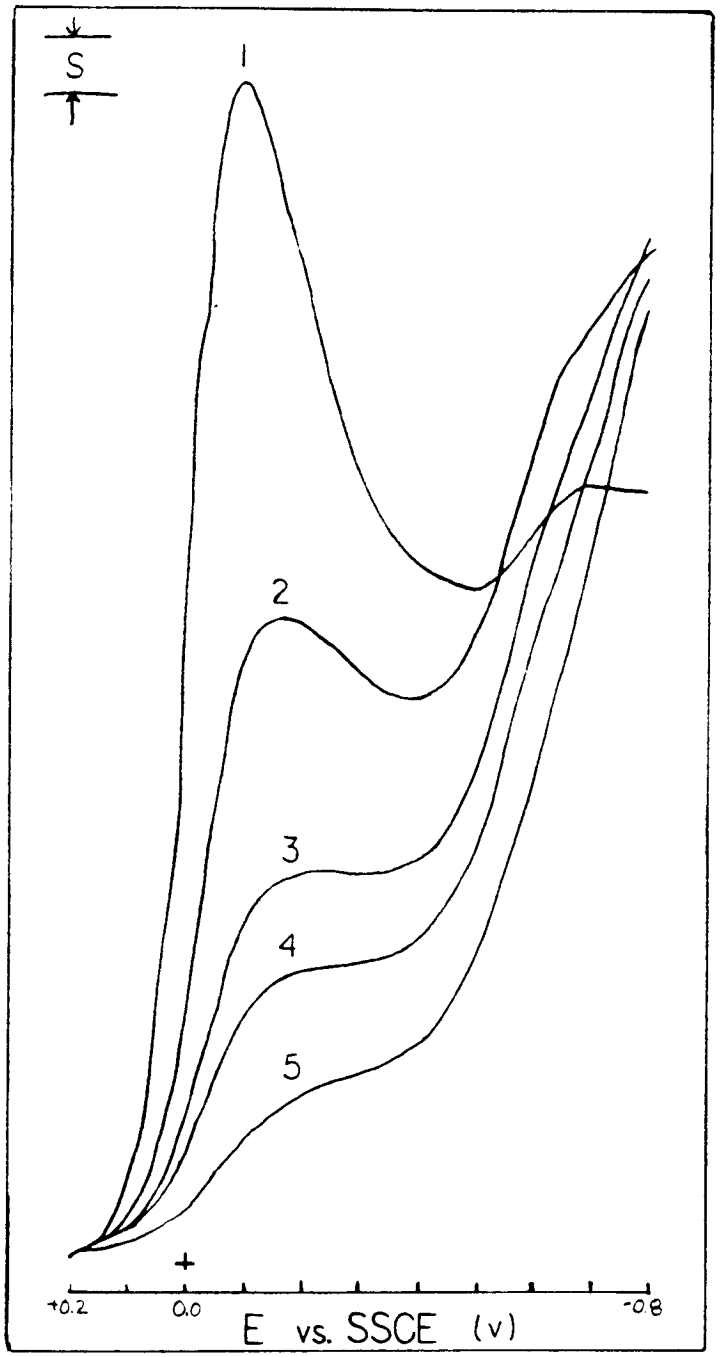

Figure 38: Loss of catalytic activity shown in successive scans 1-5.

5. CONCLUSIONS

Hydrodynamically modulated rotating disk electrodes are useful in reducing complications due to background currents. Widely applicable limits are found when testing for the loss of hydrodynamic steady-state. Many investigators have shown HMRDE to be useful in a variety of instances.[4-16] As presented in this report, the sine wave and square wave applications are cumbersome and highly inefficient. It is intended to use the IBM 9000H for the control of experimental conditions and as a collector of data. Once this is accomplished, the technique of HMRDE will be used as an extension beyond the limitations encountered in the use of RDE.

6. REFERENCES

[1] Albery, W.J.and Hitchman, M.L., *Ring-disc Electrodes*, Clarendon Press, Oxford, 1971, Chapter 1.

[2] Bard, A.J., and Faulkner, L.R., *Electrochemical Methods*, John Wiley and Sons, NY, 1980, Chapter 8.

[3] a)Von Karman, T., *Z. Angew. Math. Mech.*, **i**, 233, 1921. b)Cochran, W.G., *Proc. Camb. Phil. Soc. Mat. Phys. Sci.*, **30**, 365, 1934. c)Riddiford, A.C., *Adv. Electrochem. Electrochem. Eng.*, **4**, 47, 1966. d)Benton, E.R., *J. Fluid Mech.*, **24**, 781, 1966.

[4] Miller, B., Bellavance, M.I., and Bruckenstein,S., *Anal. Chem.*, **44**(12), 1983, 1972.

[5] Bruckenstein, S., Bellabance, M.I., Miller, B. *J. Electrochem. Soc.*, **120**(10), 1351, 1973.

[6] Miller, B. and Bruckenstein, S., *J. Electrochem. Soc.*, **121**(12), 1558, 1974.

[7] Miller, B. and Bruckenstein, S., *Anal. Chem.*, **46**(13), 2026, 1974.

[8] Tokuda, K., Bruckenstein, S., and Miller, B., *J. Electrochem. Soc.*, **122**(10), 1316, 1975.

[9] Bruckenstein, S. and Miller, B., *Accounts of Chemical Research*, **10**, 54, 1977.

[10] Tokuda, K. and Bruckenstein, S., *J. Electrochem. Soc.*, **126**(3), 431, 1979.

[11] Kenzaki, Y. and Bruckenstein, S., *J. Electrochem. Soc.*, **126**(3), 437, 1979.

[12] Blaedel, W.J. and Engstron, R.C., *Anal. Chem.*, **50**(3), 476, 1978.

[13] Blaedel, W.J. and Wang, J., *Anal. Chem.*, **52**(1), 76, 1980.

[14] Wang, J. *Talanta*, **28**, 369, 1981.

[15] Rosamilia, J.M. and Miller B., *Anal. Chem.*, **55**, 1142, 1983.

[16] Austin, D.S., Johnson, D.C., Hines, T.G. and Berti, E.T., *Anal. Chem.*, **55**, 2222, 1983.

[17] Shigehara, K., Oyama, N. and Anson, F.C., *Inorganic Chem.*, **20**, 518, 1981.

[18] Liu, H. and Anson, F.C., submitted for publication.

[19] Tsou, Y. and Anson, F.C., *J. Electrochem. Soc.*, **131**(3), 595, 1984.

[20] Shigehara, K. and Anson, F.C., *J. Phys. Chem.*, **86**, 2776, 1982.

Appendix 1: CALIBRATION OF EQUIPMENT

7.1 Sine wave

Amplitude of sine wave (volts)	DC signal of RMS-to-DC converter (volts)	Conversion factor (ratio of sine wave amplitude to dc signal)
3.0	1.04	2.88
2.0	0.68	2.94
1.0	0.34	2.94
0.5	0.168	2.98
0.3	0.104	2.88
0.1	0.034	2.94
0.05	0.017	2.94

Figure 39: Conversion factor of rectifier: 2.93 ± 1.2%

7.2 Square wave

Initial value of potential (volts) *	Final value of potential (volts) **	Ratio of final to initial
0.807	0.828	1.025
0.899	0.920	1.023
0.990	1.014	1.024
1.000	1.040	1.040
1.499	1.575	1.051
3.240	3.400	1.049
3.590	3.763	1.048
3.940	4.125	1.047

Figure 40: Conversion factors for Tektronix 5223 digitizing oscilloscope. The conversion factor used was recorded on the day of the experiment for that particular experiment. * generated from a PAR 175 Universal Programmer; ** signal has passed through the dual hi/low filter and the Tektronix digitizing scope and recorded on the XY recorder.

7.3 Rotator calibration

Dial reading (rpm)	Velocity (rpm) *	Voltage (volts) **
400	402	0.400
900	905	0.901
1600	1607	1.600
2500	2508	2.51
3600	3605	3.60
4900	4906	4.90
6400	6402	6.38
8100	8103	8.07

Figure 41: Pine Instruments MSR Rotator: velocity (rpm) = 1003.68 x voltage - 3.4208. * measured with a photo-tachometer; ** output of rotator measured with a voltmeter (1 volt = 1000 rpm).

Appendix 2: SINE WAVE MODULATION

8.1 Theoretical A values

p factor	$A_{theoretical}$
0.05	0.9537
0.10	0.8444
0.15	0.7162
0.20	0.5974
0.25	0.4972
0.30	0.4159
0.40	0.2984
0.50	0.2222
0.60	0.1714
0.70	0.1369
0.80	0.1112
0.90	0.0928
1.00	0.0792

Figure 42: Values of A for values of p factor for Sc = 1600.[8]

8.2 Variation of f and ω

ω_0 (rpm)	Amplitude of sine wave (rpm)	$i_{limiting}$ (μA)	Frequency of modulation (Hz)	$A_{experimental}$	$A_{theoretical}$	Δi_{raw} (μA)	$\Delta i_{adjusted}$ (μA)
900	180	93	2.0	0.663	0.7675	6.30	8.21
			4.0	0.424	0.4647	3.98	8.56
			6.0	0.290	0.2984	2.70	9.05
			8.0	0.190	0.2070	1.76	8.50
			10.0	0.137	0.1473	1.26	8.55
1600	320	120	2.0	0.833	0.8991	9.96	11.1
			4.0	0.662	0.7162	7.84	11.0
			6.0	0.524	0.5473	6.26	11.4
			8.0	0.409	0.4159	4.83	11.6
			10.0	0.312	0.3278	3.74	11.4
2500	500	146	2.0	0.892	0.9555	13.3	14.0
			4.0	0.804	0.8531	12.0	14.1
			6.0	0.705	0.7316	10.2	13.9
			8.0	0.596	0.6164	8.68	14.1
			10.0	0.517	0.5172	7.47	14.5
3600	720	178	2.0	0.919	0.9694	16.3	16.8
			4.0	0.861	0.9165	15.2	16.6
			6.0	0.770	0.8444	13.6	16.1
			8.0	0.721	0.7675	12.8	16.6
			10.0	0.671	0.6687	11.9	17.8
4900	980	220	2.0	0.902	0.9777	19.8	20.2
			4.0	0.855	0.9546	18.8	19.6
			6.0	0.815	0.9034	17.9	19.8
			8.0	0.735	0.8488	16.1	19.0
			10.0	0.635	0.7880	13.9	17.7
6400	1280	240	2.0	0.949	0.9824	22.7	23.1
			4.0	0.919	0.9653	22.0	22.8
			6.0	0.766	0.9406	18.3	19.5
			8.0	0.674	0.8991	16.1	17.9
			10.0	0.551	0.8575	13.2	15.4

Figure 43: Frequency and rotational variation data. Reagent concentration: 1 mM $K_3Fe(CN)_6$; supporting electrolyte concentration: 0.1 M KCl; working electrode: Pine pyrolytic graphite (Ar=0.196 cm^2); counter electrode: platinum; reference electrode: SSCE; Sc = 1600.

$$\Delta i_{adjusted} = \frac{1}{A_{theory}} \times \Delta i_{raw}$$

$$A_{experimental} = \frac{\Delta i_{raw}}{i_{limiting} \times \frac{\Delta\omega^{1/2}}{\omega^{1/2}}}$$

$A_{theoretical}$: from section 1 of Appendix 2

$$\frac{\Delta\omega^{1/2}}{\omega^{1/2}} = 0.10$$

8.3 Amplitude variation

ω_0 (rpm)	Frequency of modulation (Hz)	p factor	$A_{theoretical}$	$i_{limiting}$	Amplitude of sine wave (rpm)	$\frac{\Delta\omega^{1/2}}{\omega^{1/2}}$	Δi_{raw}	$\Delta i_{adjusted}$	$A_{experimental}$
900	6.0	0.4	0.2984	94	90	0.0333	1.24	4.16	0.401
					120	0.0667	1.67	5.60	0.267
					160	0.0890	2.42	8.11	0.287
					180	0.100	2.70	9.05	0.291
					200	0.111	3.08	10.3	0.293
					300	0.167	4.66	15.6	0.295
					360	0.201	5.49	18.4	0.289
1600	6.0	0.225	0.5473	120	80	0.025	1.47	2.68	0.490
					160	0.050	3.08	5.62	0.515
					320	0.100	6.26	11.4	0.524
					480	0.150	9.30	17.0	0.519
					640	0.201	12.5	22.9	0.521
2500	6.0	0.144	0.7316	150	125	0.025	2.64	3.60	0.706
					250	0.050	5.20	7.11	0.696
					500	0.100	10.2	13.9	0.705
					750	0.150	16.1	22.0	0.719
					1000	0.201	21.0	28.6	0.697
3600	6.0	0.10	0.8444	180	100	0.0139	1.57	1.87	0.632
					200	0.0278	3.66	4.34	0.734
					360	0.0500	6.74	7.98	0.751
					600	0.0834	11.0	13.0	0.734
					720	0.100	13.6	16.1	0.770
					800	0.111	15.6	18.5	0.784
					1000	0.139	19.7	23.3	0.790
					1200	0.167	23.8	28.2	0.817
					1400	0.195	27.7	32.8	0.814
					1500	0.209	27.5	32.6	0.756
					2000	0.281	35.7	42.3	0.718
					2500	0.353	46.5	55.1	0.750
					3000	0.426	54.0	64.0	0.727
4900	4.0	0.049	0.9546	220	240	0.0245	4.47	4.68	0.832
					490	0.0500	9.52	9.98	0.869
					980	0.100	18.8	19.6	0.855
					1500	0.154	30.5	31.9	0.902
					2000	0.205	41.0	43.0	0.913
6400	2.0	0.019	0.9824	240	320	0.025	5.27	5.36	0.882
					640	0.050	11.1	11.3	0.931
					1280	0.100	22.7	23.1	0.946

Figure 44: Amplitude variation data. Reagent concentration: 1 mM $K_3Fe(CN)_6$; supporting electrolyte concentration: 0.1 M KCl; working electrode: Pine pyrolytic graphite (Ar=0.196 cm^2); counter electrode: platinum; reference electrode: SSCE; Sc = 1600.

$$\Delta i_{adjusted} = \frac{1}{A_{theory}} \times \Delta i_{raw}$$

$$A_{experimental} = \frac{\Delta i_{raw}}{i_{limiting} \times \Delta \frac{\omega^{1/2}}{\omega^{1/2}}}$$

$A_{theoretical}$: from section 1 of Appendix 2

p factor	$A_{experimental}$	$A_{theoretical}$
0.400	0.287 ± 3.6%	0.2984
0.225	0.514 ± 2.7%	0.5473
0.144	0.705 ± 1.3%	0.7316
0.100	0.752 ± 6.4%	0.8444
0.049	0.866 ± 4.9%	0.9546
0.019	0.919 ± 3.6%	0.9824

Figure 15: Amplitude variation data.

ω_c (rpm)	$i_{limiting}$ (μA)	Frequency of modulation (Hz)	Δi_{raw}	$A_{experimental}$ (μA)
900	98.8	1.50	8.72	0.793
1600	129	2.67	11.3	0.790
2500	160	4.17	14.3	0.802
3600	190	6.0	17.4	0.824
4900	218	8.17	20.0	0.826
6400	255	10.7	20.2	0.711

Figure 46: Constant p factor data. Reagent concentration: 1 mM $K_3Fe(CN)_6$; supporting electrolyte concentration: 0.1 M KCl; working electrode: Pine pyrolytic graphite (Ar=0.196 cm^2); counter electrode: platinum; reference electrode: SSCE.

$$\frac{\Delta\omega^{1/2}}{\omega^{1/2}} = 0.10$$

$$A_{experimental} = \frac{\Delta i_{raw}}{i_{limiting} \times \Delta \frac{\omega^{1/2}}{\omega^{1/2}}}$$

$A_{theoretical}$: 0.8444

p factor = 0.1

Appendix 3: SQUARE WAVE DATA

9.1 Rotational rate variation

ω_0 (rpm)	$\Delta\omega^{1/2}$ (rpm$^{1/2}$)	$i_{limiting}$ (μA)	Δi_{raw} (μA)	$\Delta i_{calculated}$ (μA)
1600	320	127	12.2	11.9
2500	500	158	15.0	14.8
3600	720	186	18.2	18.0
4900	980	215	21.0	21.0
6400	1280	245	23.5	24.0

Figure 47: Rotational rate variation. Reagent concentration: 1 mM $K_3Fe(CN)_6$; supporting electrolyte concentration: 0.1 M KCl; working electrode: Pine pyrolytic graphite (Ar=0.196 cm^2); counter electrode: platinum; reference electrode: SSCE; potential = -0.10 volts; frequency = 0.10 Hz, Sc = 1600.

$$\Delta i_{calculated} = \frac{\Delta\omega^{1/2}}{\omega^{1/2}} \times i_{limiting}$$

9.2 Frequency variation

ω_0 (rpm)	$\Delta\omega^{1/2}$ (rpm$^{1/2}$)	frequency of modulation (Hz)	p factor	$\Delta i_{adjusted}$ (μA)	A
900	180	0.1	0.0065	9.5	1.00
		0.5	0.032	9.2	0.97
		1.0	0.065	9.3	0.98
		2.5	0.16	7.0	0.74
		5.0	0.32	4.0	0.42
		10.0	0.65	1.8	0.19
2500	500	0.1	0.0024	14.7	1.00
		0.5	0.012	14.4	0.98
		1.0	0.023	13.8	0.94
		5.0	0.12	13.5	0.92
		10.0	0.23	8.5	0.58

Figure 48: Frequency variation. Reagent concentration: 1 mM $K_3Fe(CN)_6$; supporting electrolyte concentration: 0.1 M KCl; working electrode: Pine pyrolytic graphite (Ar=0.196 cm^2); counter electrode: platinum; reference electrode: SSCE; potential = -0.10 volts; Sc = 1600.

$$\frac{\Delta\omega^{1/2}}{\omega^{1/2}} = 0.10$$

$$A = \frac{i \times Hz}{i \times 0.1\ Hz}$$

$$\Delta i_{adjusted} = \frac{\Delta i_{raw}}{1.034} \text{ (scope compensation)}$$

9.3 Amplitude variation

$\Delta\omega^{1/2}$ (rpm$^{1/2}$)	$\Delta\omega^{1/2}/\omega^{1/2}$	Δi_{raw} (μA)	$\Delta i_{calculated}$ (μA)
2.48	0.0824	7.70	7.40
3.01	0.100	9.60	9.00
4.65	0.155	14.7	13.8
5.98	0.199	19.1	17.8
9.10	0.302	28.5	27.0

Figure 49: Amplitude variation. Reagent concentration: 1 mM $K_3Fe(CN)_6$; supporting electrolyte concentration: 0.1 M KCl; working electrode: Pine pyrolytic graphite (Ar=0.196 cm^2); counter electrode: platinum; reference electrode: SSCE; potential = -0.10 volts; Sc = 1600; ω_0 = 900 rpm; frequency of modulation = 0.10 Hz; p factor = 0.0065; $i_{limiting}$ = 97.3μA.

$$\Delta i_{calculated} = \frac{\Delta\omega^{1/2}}{\omega^{1/2}} \times i_{limiting}$$